FINAL MASTER THESIS

ERASMUS Mundus Master's Degree
in Hydrogen System and Enabling Technologies
(HySET)

Advancing Overpressure Quantification Methodology for Hydrogen Venting

Report and Appendices

Author:	Adisa Jarubenjaluk
UPC Supervisor:	Asst. Prof. Pascale Vacca
Department	Department of Chemical Engineering
PoliTo Supervisor:	Assoc. Prof. Andrea Carpignano
Industrial Supervisor:	Dr. Josué Melguizo-Gavilanes
Call:	June 2025

Abstract

A major safety problem at present is the lack of an agreed methodology to estimate blast loads from hydrogen (H_2) vents. Of particular interest is the delayed ignition of the flammable clouds that form upon a controlled or uncontrolled release. This study aims to test and improve an existing methodology to enable more accurate prediction of overpressure in hydrogen venting scenarios. Present deflagration model underestimates overpressures by an order of magnitude, whereas the detonation model results in overly conservative estimates albeit useful to retain as an upper limit. While in safety assessments, a certain degree of conservatism is preferred due to the non-negligible potential consequences, estimates should be realistic and in line with the physics that expected to play a role emphasising the need to improve deflagration modelling. Visible flame speed is identified as the most influential parameter in the deflagration model. Modelled estimates based on cloud radius tends to yield slower flame speeds. An alternative approach using the Reynolds number—reflecting the turbulence induced by pressurised gas release—was proposed. The refined methodology was tested against vertical hydrogen release experiments, demonstrating an improvement in overpressure predictions from 13% using the original methodology to 73% of the predictions falling within a factor of four overestimation.

Resum

Un problema de seguretat clau és la manca d'un mètode estàndard per estimar les càrregues d'explosió derivades de respiradors d'hidrogen, especialment quan hi ha ignició retardada després d'una alliberació. Aquest estudi prova i refina una metodologia existent per predir millor la sobrepressió durant la ventilació d'hidrogen. Els models de deflagració actuals subestimen notablement la sobrepressió, mentre que els de detonació són excessivament conservadors però útils com a límit superior. Tot i que el conservadorisme és habitual per seguretat, les prediccions han de ser realistes i coherents amb la física esperada. Per això cal millorar la modelització de la deflagració. La velocitat de la flama és el paràmetre més influent, i les estimacions basades en el radi del núvol tendeixen a donar velocitats més lentes. Es proposa un enfocament alternatiu basat en el nombre de Reynolds, que reflecteix la turbulència causada per l'alliberament de gas a pressió. La metodologia refinada es va provar amb experiments d'alliberament vertical d'hidrogen, demostrant una millora en les prediccions de sobrepressió: del 13 % amb la metodologia original al 73 % de les prediccions dins d'un factor quatre de sobreestimació.

Resumen

Un problema clave de seguridad es la falta de un método estándar para estimar las cargas de explosión de ventilaciones de hidrógeno, especialmente cuando ocurre una ignición retardada tras la liberación. Este estudio prueba y mejora una metodología existente para predecir mejor la sobrepresión en estos escenarios. Los modelos actuales de deflagración subestiman significativamente la sobrepresión, mientras que los de detonación resultan excesivamente conservadores, aunque útiles como límite superior. Aunque el conservadurismo es común en evaluaciones de seguridad, las estimaciones deben ser realistas y coherentes con la física implicada. Mejorar la modelización de la deflagración es, por tanto, esencial. La velocidad de la llama es el parámetro más influyente, y los cálculos basados en el radio del núcleo tienden a dar velocidades más bajas. Se propone un enfoque alternativo basado en el número de Reynolds, que refleja la turbulencia provocada por la liberación de gas a presión. La metodología refinada se probó frente a experimentos de liberación vertical de hidrógeno, demostrando una mejora en las predicciones de sobrepresión: del 13 % con la metodología original al 73 % de las predicciones dentro de un factor cuatro de sobreestimación.

Acknowledgement

To begin with, I would like to mention the HySET Erasmus Mundus Master programme, which has played a key role in connecting universities with industry and ultimately brought me to this point. Academically, my journey was shaped by Politecnico di Torino (PoliTo) and Universitat Politècnica de Catalunya (UPC), who jointly supervised my thesis in collaboration with Shell. This partnership added valuable real-world experience to my academic work.

I would like to express my deepest gratitude to all those who supported me throughout my thesis journey—from the very beginning to the final stages.

First and foremost, I would like to thank Josué Melguizo-Gavilanes, my Shell supervisor, for his patience, guidance, and support throughout every stage of this thesis. I am truly grateful for the sincere commitment you showed in supervising my work. Your advice and encouragement—both academically and personally—have helped me grow, develop, and move forward in meaningful ways.

I am also thankful to Professor Pascale Vacca from UPC and Professor Andrea Carpignano from Politecnico di Torino for their valuable time and insightful guidance in shaping this thesis. Your suggestions made a real impact.

A special thank you goes to Evren Unsal, Shell's academic partnerships manager, for your continuous support in creating opportunities for students like me to carry out a thesis project with Shell experts. Without you, this master's thesis would not have existed. Your positivity and dedication to making us feel supported as interns made this journey enjoyable.

I'm also grateful to my family, friends, and fellow interns at Shell. Your kindness, patience, and support helped me through all the ups and downs. A big thank you as well to the many amazing people I met during this master thesis period—your advice on study, work, and career has truly stayed with me.

Although words may not fully capture how grateful I feel, I sincerely thank everyone who has been part of this journey. Your guidance, help, and encouragement have brought me to this point of achievement.

Table of Contents

List of Tables

List of Figures

List of abbreviations

BS	Baker-Strehlow
BST	Baker-Strehlow-Tang
CFD	Computational Fluid Dynamics
DDT	Deflagration-to-Detonation Transition
FCP	Fundamental Combustion Properties
FRED	Fire Release Explosion Dispersion
H_2	Hydrogen
HDPE	High-density Polyethylene
LFL	Lower Flammability Limit
LHV	Lower Heating Value
MCA	Manufacturing Chemists' Association
PHAST	Professional, Process Hazard Analysis Software Tool
TNT	Trinitrotoluene
VCE	Vapor Cloud Explosion

1 Introduction

Annual growth in global hydrogen (H_2) demand is expected year-on-year [2]. While hydrogen is not a new material, it is expected to remain critical, especially in industrial facilities, to ensure the safe handling of hydrogen. Safety protocols are mandatory for all facilities that handle hydrogen, such as hydrogen production sites or storage and handling facilities, to ensure safe operation during regular operational demands, maintenance, and emergencies scenarios. This work will focus on hydrogen vent systems in which hydrogen is released through a circular opening at the vent header. The sections below introduce the scope of hydrogen venting and the associated challenges.

1.1 Hydrogen venting

To ensure a well-defined scope of interest depending on the venting application, the release scenarios are categorised according to vent diameter (of the circular opening) and release pressures into: (i) process venting and (ii) typical hydrogen storage venting. In process venting, large vent diameters and low release pressures are expected, whereas in hydrogen storage applications, higher release pressures and smaller vent diameters are anticipated. The primary parameter ranges are listed in the table below and serve as a starting point of the study.

Table 1 Scope of venting based on different applications

	Process venting	**H_2 storage**
Vent diameter	300–600 mm	4–52 mm
Vent release pressure	1.3–2 bara	100–1000 bara

Due to lack of an agreed-upon approach for estimating blast overpressure specifically for large-scale venting and the increased relevance and demand from industries building and planning to operate large hydrogen facilities, there is a pressing need to have standard protocols to quantify potential hazards, especially overpressure. Thus, the initial focus of the study is on the range of process venting.

To illustrate a possible configuration of an industrial-scale hydrogen vent, an AI-generated image (Figure 1) is used, as no published design is currently available.

Figure 1 Schematic of what a hydrogen vent stack might look like in a large-scale industrial setting, generated by ChatGPT.

1.2 Challenges associated with hydrogen venting

Hydrogen venting prevents over-pressurisation and ensures the process safety [3], encompassing pressure relief lines, boil-off from cryogenic systems, and hydrogen purged during maintenance processes. Proper vent design is a key to prevent cloud formation and reduce the potential for delayed ignition. Even though hydrogen disperses quickly due to its low molecular weight and high diffusivity, reducing its risk of accumulation [4], adequate protocols are necessary for safe discharge of unused hydrogen at locations away from personnel, facilities and nearby habitants.

Key challenges in hydrogen venting include: (i) prediction of dispersion patterns under variation of factors such as environmental conditions (i.e. wind speed and direction, ambient temperature, and humidity), released inventory, and vent geometry; and (ii) preventing the risk of hydrogen ignition.

The gas cloud dispersion can be studied using standard consequence analysis tools such as PHAST (Professional, Process Hazard Analysis Software Tool) and Shell FRED (Fire Release Explosion Dispersion), which will be further discussed in the methodology section.

However, mitigation of hydrogen cloud ignition to avoid jet fire and explosion scenarios is more challenging. Hydrogen is prone to immediate ignition or ignition after a time delay following the start of release—due to its high reactivity, low ignition energy (<0.03 mJ, whereas static electricity from the human body can reach 8.33 mJ), and wide flammability range (ca. 4% to 75% by volume hydrogen-air mixture) [5]. Several incidents involving spontaneous hydrogen ignition have been reported in the literature [6,7]. Once a vented hydrogen cloud is ignited, it can lead to fire and explosion accidents, posing both thermal and, more critically, overpressure hazards due to hydrogen's high burning rate under turbulent conditions [7,8]. This raises an important question: if a dispersed flammable cloud ignited, how can the consequences caused by the venting of hydrogen be properly assessed and mitigated?

Existing industrial standards, such as API 521 [9], indicate vent design guidelines to reduce thermal radiation risks, but they do not cover the overpressure hazards resulting from vent releases. Although venting gas at a certain height above the ground can help reduce the thermal hazard to personnel, there are still unknown overpressure risks if workers are standing in proximity to the vent stack and ignition of the flammable gas occurs close. The need to reliably estimate overpressure effects for hydrogen venting scenarios to assess potential consequences—based on both normal operating conditions and worst-case events—is crucial for implementing proper safety mitigations and measures.

Studies have explored approaches for estimating blast loads from unconfined and uncongested hydrogen releases, including performing large-scale experiments, CFD simulations, and applying existing simplified models. Currently, due to limited availability of large-scale experiments, modellings are becoming more attractive choice.

CFD is not preferred in industry due to its high computational cost and long simulation times required to account a wide range of release scenarios [10]. Empirical models such as the TNT equivalency *[11]*, the TNO multi-energy [12], and the Baker-Strehlow models [13,14] have demonstrated reliability for conventional hydrocarbons, but they have been shown to perform poorly when applied to hydrogen [15,16].

Therefore, this study adopts the methodology proposed by Melguizo-Gavilanes et.al. [1] which comprises of two modelling stages: (i) a dispersion calculation and (ii) the use of overpressure correlations. Based on known vent release conditions (i.e., vent diameter and vent release pressure), the dispersion model estimates the mass and volume of hydrogen gas within the cloud. These outputs then serve as inputs to the overpressure models, where overpressures are computed using deflagration and detonation correlations first introduced by Dorofeev [17].

The methodology is first validated against available large-scale experimental data to evaluate its predictive performance for unconfined and uncongested hydrogen releases. It was found that the deflagration and detonation overpressure correlations tend to underpredict and overpredict the

overpressures by an order of magnitude, respectively. A conservative yet realistic estimation is favoured in the field of safety, highlighting the importance of refining the deflagration model. Among all inputs to the deflagration correlation, the visible flame speed is the most critical factor in overpressure prediction. With the current approach, flame speed estimates are typically significantly underestimated. To improve these estimates, an enhanced methodology is proposed that incorporates a scaling approach relating vent release conditions (i.e., vent diameter and release pressure) to the visible flame speed. This enhancement leads to more accurate overpressure predictions when validated against experimental data. These improved estimates are subsequently translated into potential consequences in terms of the severity of damage, injury, or fatality associated with given release conditions.

2 Background and literature review

This section includes a review of past accidents and their consequences involving hydrogen releases without congestion or confinement, corresponding to the hydrogen venting scenario. It is followed by an introduction to the fundamental combustion regimes—deflagration and detonation— relevant to situations involving delayed ignition of a released hydrogen cloud. State-of-the-art overpressure quantification approaches are described, and existing knowledge gaps are identified.

2.1 Current knowledge in hydrogen venting

Historically, the knowledge surrounding hydrogen venting accidents has been limited. Thomas et.al. [18] listed incidents involving unconfined hydrogen vapor cloud explosion (VCE) up to the year of publication, 2015. The reported consequences of those incidents were often severe, ranging from minor to extensive property damage, injuries, and in the worst case, fatalities. Only a few reviewed cases were hydrogen venting relevant, that is unconfined and uncongested hydrogen releases. Therefore, the summary here includes the Jackass Flats incident, the Manufacturing Chemists' Association (MCA) case history and NASA H_2 incidents.

In the Jackass Flats incident [19,20], hydrogen was one of several fuels tested with the rocket motors to assess resulting noise levels, without intentional ignition. Hydrogen gas was released vertically into the open atmosphere through a nozzle for 13 seconds before autoignition occurred. The VCE was documented as a deflagration, involving an estimated 90 kg or 10% of the total hydrogen released, contributing to the explosion. The incident led to minor damage to the surrounding buildings.

Another accident reported in the work of Thomas et.al. [18], the MCA case, involved an explosion resulting from hydrogen gas released through a vent stack. However, no data on the release quantity, ignition time delay or overpressure were provided. The consequences were described as severe damage to buildings in vicinity of facility.

More accidents can be found in the report by Ordin [21], which documented 96 hydrogen-related accidents during NASA operations involving both intentional and unintentional hydrogen releases. The report included brief descriptions of the fire and explosion accidents and their causes, but not all entries provided comprehensive information, such as release quantities, resulting overpressures, or impacts on property or personnel.

Two clear cases of unconfined and uncongested hydrogen releases from the NASA report are worth mentioning [21]. In one incident, hydrogen gas was released into the open air, followed by self-ignition and an explosion near a hydrogen vent stack after normal operations. Neither the release quantity nor consequences were reported. However, a similar incident occurred at another test facility involved also the venting of a significant quantity of hydrogen gas, which was unintentionally ignited and exploded near the vent stack. This incident caused damage to the test area, though no injuries or fatalities were mentioned. In both cases, the ignition sources could not be identified. Based on this NASA report [21], such incidents are not uncommon when hydrogen is released into the open air; 66 out of 96 mishaps involved hydrogen releases to the atmosphere. Of these, 41 resulted in ignition, and in 36% of those cases, the ignition source remained unidentified. The remaining ignited cases were attributed to weak ignition sources such as sparks or static charges. This highlights how easily hydrogen can be ignited. Furthermore, it is observed that both venting incidents occurred under calm weather conditions or no wind. The probable effect was mentioned to be hydrogen gas did not disperse quickly, allowing the formation of an ignitable gas cloud before ignition. This report also reflects the complications that external environmental factors pose for hydrogen venting, particularly when dispersion is limited, allowing the accumulation of flammable hydrogen–air clouds.

According to reported accidents, it is evident that unconfined and uncongested hydrogen releases pose risks of fire and severe explosions. However, the potential hazards associated with such releases are still underestimated by industry [18]. In contrast, confined hydrogen releases—e.g., within

enclosures with roofs and walls—are widely acknowledged to pose significant explosion risks. Therefore, it is essential for research to enable accurate estimation of the consequences, i.e., thermal and overpressure hazards, of hydrogen releases under various conditions. One important aspect this study examines is the magnitude of overpressure resulting from hydrogen vent releases upon delayed ignition of the flammable cloud, based on the two combustion regimes: deflagration and detonation.

2.2 Deflagration vs detonation

Deflagration and detonation are two distinct combustion modes, characterised by different propagation physics. Deflagration is driven by molecular heat and mass transfer whereas detonation is driven by shock-induced ignition, which leads to drastic change in thermodynamic properties, such as pressure and temperature within the combustion system [22]. To initiate deflagration and detonation, an ignition source and a flammable mixture with an appropriate ratio of fuel and oxidizer are required.

Figure 2 and Figure 3 show the initiation and propagation of a deflagration and detonation, respectively. These two phenomena can be distinguished based on a few observations. Deflagration starts with the weak ignition of a combustible mixture (for example, an electrical spark igniter can generate energy of 100 mJ [7]), producing a reaction front that travels at subsonic speed, relative to a fixed observer. In contrast, direct detonation requires a high-energy ignition source, such as the C-4 high explosive used in Groethe et.al. (2007) [7] to ignite a 300 m^3 30% H_2/air mixture, generating spherical shock waves and flame front that propagate together at supersonic speeds—on the order of thousands of meters per second. The difference in wave propagation speed can be clearly observed by comparing the time stamp in Figure 2 and Figure 3, with the latter being a thousand times faster. Besides the variation in propagation speed, the resulting pressure across the wave front also differs. Detonation generates much higher overpressures and more severe consequences than deflagration under the same conditions [5,22].

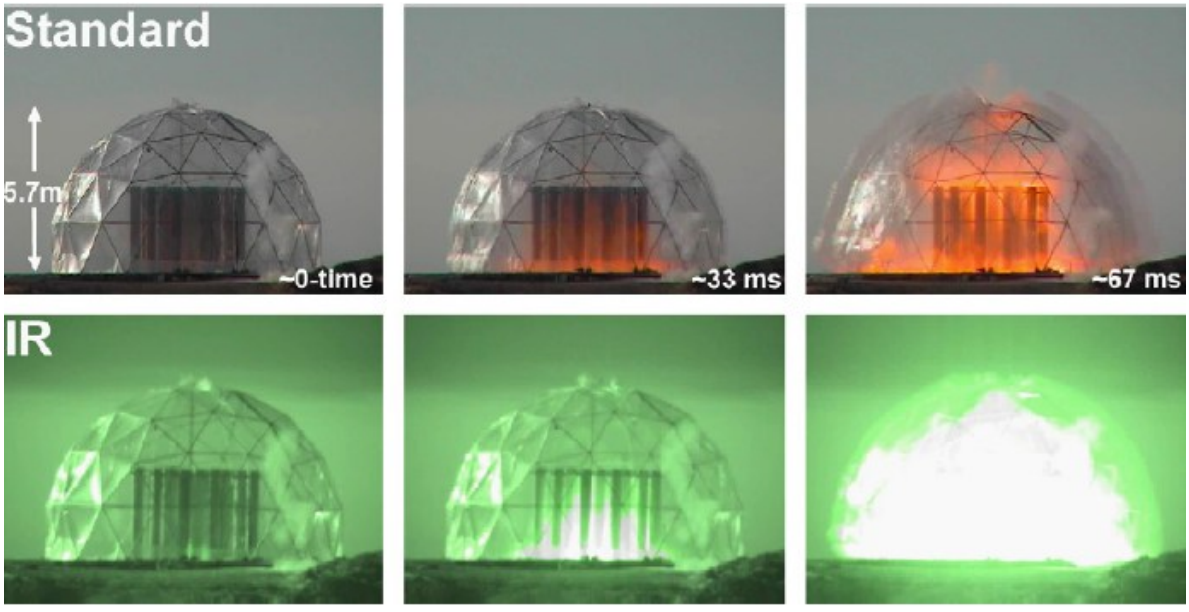

Figure 2 Standard and infrared video frames of a 300-m^3 hemispherical high-density polyethylene (HDPE) dome used for a deflagration test, containing 30% H_2/air with eight cylinders as obstacles [7]. The HDPE was cut just before ignition, which was initiated at the bottom centre of the hemisphere using a spark.

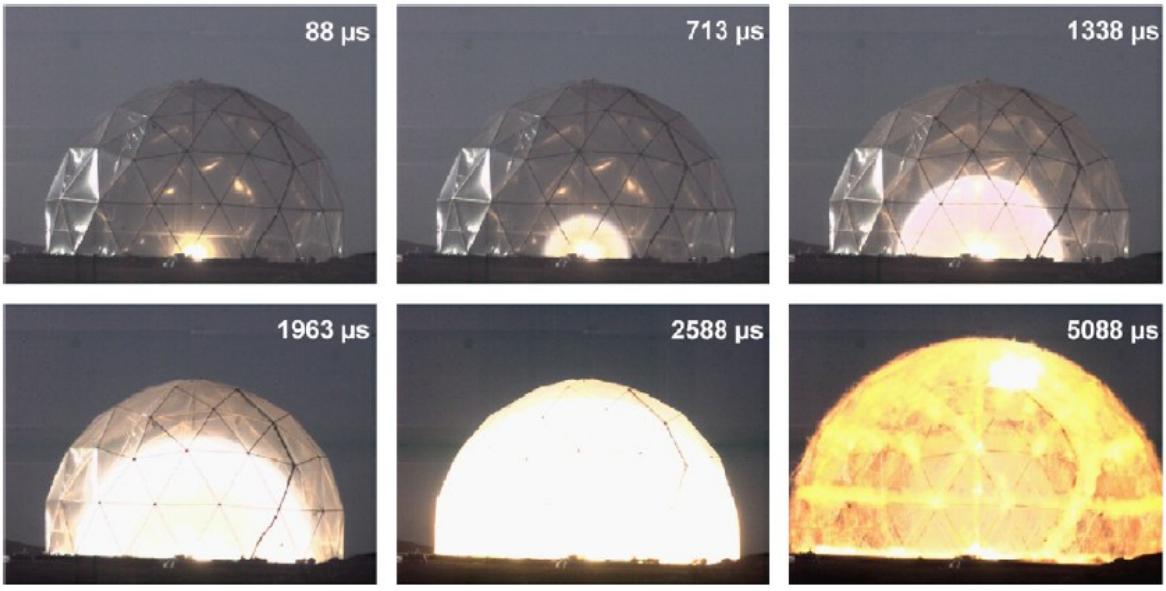

Figure 3 High-speed video frames of a 300-m^3 detonation experiment containing stoichiometric concentration of H_2/air in HDPE hemispherical dome [7]. The ignition was initiated at the bottom centre of the hemisphere using C-4 high explosive.

Apart from direct initiation, another potential route to initiate a detonation is via flame acceleration within the flammable cloud. In a venting situation where the release of a hydrogen jet ignites after a delay, either through ignitors or other external sources like static build-up and autoignition, the flame can undergo acceleration and then subsequentially transition to an explosion under the right conditions. This process is known as deflagration-to-detonation transition (DDT). Two flame acceleration mechanisms under unconfined and uncongested releases are possible: (i) intrinsic flame instabilities and (ii) self-turbulisation due to the interaction between the flame and turbulent flow generated by the releases [23]. Although the flame acceleration is acknowledged to be more critical in the presence of confinement and congestion [5,17], even in open environments, DDT remains a possibility that must be considered, as it can lead to catastrophic consequences. As a result, the adequate estimation of overpressure from hydrogen venting shall take into account both deflagration and detonation loads for a given release condition, defining a range of possible consequences, with deflagration and detonation providing lower and upper bounds, respectively.

2.3 Conventional approaches to quantifying blast overpressure

Readdressing the focus of the research problem in this project, which is how to predict deflagration and detonation overpressure associated with unconfined and uncongested hydrogen releases, literature has illustrated numerous methodologies, including experimental studies, computational fluid dynamics (CFD) modelling, and the use of existing simplified VCE correlations, such as the trinitrotoluene (TNT) equivalency, TNO multi-energy, Baker-Strehlow (BS), Baker-Strehlow-Tang (BST) methods [5,10–16,24,25].

There is limited publicly available information on such large-scale hydrogen experiments, particularly involving vertical releases without congestions and confinements. Achieving reliable predictions of large-scale incidents by scaling up the phenomena from small-scale experiments is unlikely, as this approach could not represent real situations accurately [7]. This is due to differences in characteristics of the physical event at operational scale that may be excluded in small-scale experiments [5,24]. Therefore, there is a need for at-scale experimental data to better understand the occurrence of deflagration and detonation phenomena. However, given an urgency to quantify the overpressure effect, modellings became more attractive choices.

CFD is not an ideal tool for modelling large-scale incidents due to its high cost and long computation times required to simulate combination of all release scenarios [10]. In addition, the prediction accuracy varies and requires further validation [25]. Similarly, the challenge of limited large-scale experimental data, as mentioned earlier, makes it more difficult to improve and revalidate these CFD models.

Another option is the computation of overpressure using existing empirical models of vapour cloud explosions for hydrogen releases. These correlations already exist and are valid for conventional hydrocarbon fuels, including the TNT equivalency, TNO multi-energy, BS, and BST methods. The models and their suitability to hydrogen-air system are described below.

The TNT equivalency method *[11]* translates the mass of flammable gas in the cloud into equivalent TNT mass. The pressure build-up is then estimated by the scaled distance. The expressions are as follows:

$$W_{TNT} = \eta \cdot \frac{M \Delta H_C}{\Delta H_{TNT}} \qquad \textit{Equation 1}$$

$$d_n = \frac{d}{W_{TNT}^{\frac{1}{3}}} \qquad \textit{Equation 2}$$

$$\frac{\Delta P}{P_0} = \frac{1}{d_n} + \frac{4}{{d_n}^2} + \frac{12}{{d_n}^3} \qquad \textit{Equation 3}$$

Where W_{TNT} is an equivalent TNT mass (kg). η is an explosion efficiency (0.46 for hydrogen-air [16]). M is a mass of flammable gas in the cloud (kg). ΔH_C is the heat of combustion of flammable gas (3420 kJ/kg for stoichiometric hydrogen-air concentration [16]). ΔH_{TNT} is the energy of explosion of TNT (4680 kJ/kg). d_n is the scaled distance (m·kg$^{-1/3}$). d is a distance from explosion centre to the point of estimated overpressure (m). P_0 is atmospheric pressure (bar). ΔP is blast overpressure (bar).

The TNT equivalency model is the least complex among the models mentioned, it computes overpressure based on only mass of the gas in the cloud and then factoring in the explosion efficiency. However, this simplified approach typically provides significantly inaccurate overpressure prediction for hydrogen-air explosion [15,16].

The TNO multi-energy method [11,12] assumes that a portion of a partially confined flammable cloud can be represented as an equivalent hemispherical cloud containing a uniform stoichiometric concentration of hydrocarbon and air (0.1 kg/m³), while the remainder of the unconfined part does not contribute to the resulting overpressure. The model's major dependency is on the confinement and congestion and places less importance on the mass of fuel in the vapour cloud. The congestion scale ranges from 1 to 10, depicting the weakest explosion (with no confinement and less congestion) to the strongest explosion (with maximum confinement and congestion), resulting in graphical models relating dimensionless parameters of blast wave properties, such as scaled peak overpressure and scaled positive phase duration, as a function of dimensionless scaled distance [12]. The expressions are as follows:

$$P^* = \frac{\Delta p}{p_0} \qquad \textit{Equation 4}$$

$$t_+{}^* = t_+ u_s \left(\frac{p_0}{E}\right)^{\frac{1}{3}} \qquad \textit{Equation 5}$$

$$R^* = R(\frac{p_0}{E})^{\frac{1}{3}} \qquad \textit{Equation 6}$$

Where $P^*, {t_+}^*$ and R^* are dimensionless Sachs scaled overpressure, positive phase duration, and distance respectively. P^* and ${t_+}^*$ can be obtained from set of curves in Van Den Berg A.C. [12]. $\Delta p = p - p_0$ is the overpressure (Pa), where p is the pressure at the point of interest (Pa) and p_0 is atmospheric pressure (Pa). t_+ is positive phase duration (s). u_s is speed of sound in air (m/s). R refers to the distance or radii from the blast epicentre (m), and E represents anticipated combustion energy released (J).

The TNO model defines the strengths of gas explosions as strongly governed by the level of confinement and congestion. It assumes that resulting overpressure is influenced by turbulence gas flow caused by obstacles and confinements. In the case, of hydrogen venting, which focuses on unconfined and uncongested explosions, this model is therefore not adequate for estimating overpressure from open-air hydrogen explosions [15].

The Baker-Strehlow (BS) method [14] estimates overpressure and generated impulse with respect to the Sachs scaled distance, based on flame speed (expressed as Mach number) obtained from literature reviews. This flame speed is considered a function of chemical reactivity, geometry, congestion, and confinement. The method also incorporates the concept of the TNO multi-energy method for determining the combustion energy released (E). As a result, a selection of blast curves is available based on different flame speeds.

The Baker-Strehlow-Tang (BST) model [13], an improved model built upon the original BS method, was proposed later in 2005. The concepts of the BST model remain similar to those of the BS method. The key changes include new sets of blast curve charts for both overpressure and impulse, as well as a revised criteria for selection of Mach numbers based on medium-scale experiments.

The expressions for Sachs scaled overpressure and distance using in BS and BST models remain the same as described in the TNO multi-energy method, while the Sachs scaled impulse is described as follows:

$$i^* = \frac{i \cdot u_s}{{p_0}^{\frac{2}{3}} \cdot E^{\frac{1}{3}}} \qquad \textit{Equation 7}$$

Where i^* is Sachs scaled impulse, obtained from scaled impulse-distance chart based on flame speed [13,14]. i is specific impulse (Pa·s).

Both BS and BST models' assumptions are also similar to those of the TNO model, as they account for congestion and confinement through the flame speed, which makes them unsuitable for representing open-air explosions [15].

To conclude this section, due to the limited availability of large-scale, unconfined, and uncongested hydrogen release experiments, there is a clear need to explore alternative methods for assessing overpressure from hydrogen venting. The large number of possible release scenarios makes CFD unsuitable for overpressure quantification at an industrial scale. Existing vapor cloud explosion (VCE) correlations are also unreliable for estimating overpressure associated with open-air hydrogen blasts for two main reasons. First, these models typically consider only the quantity of gas, without incorporating sufficient gas properties within the cloud. Second, model such as TNO, BS, BST include confinement and congestion effects, which is not in the scope of interest.

These VCE correlations are developed and validated with hydrocarbons. However, the fact that hydrogen behaves differently—as it is more reactive, more prone to ignite, and has a higher burning rate than hydrocarbons—generates discrepancies in predictions when applying these conventional models. This leads to the speculation that these empirical models are inadequate because the correlations do not sufficiently account for the different combustion properties of hydrogen gas. This highlights the need to introduce alternative methodologies that can more accurately predict

overpressure, especially given that there is currently no agreed-upon model specifically applicable to assess the overpressures resulting from delayed ignition of unconfined and uncongested hydrogen releases. This knowledge gap leads to the main purpose of this project: to introduce and improve an alternative methodology that provides accurate overpressure estimates.

3 Goal and Objectives

The goal of this study is to enhance the predictive capabilities of overpressure models for hydrogen venting during normal operation, transient and accidental scenario by revisiting the work of Dorofeev [17]. The release conditions of interest fall within the range of process venting, having a combination of vent diameter and pressure in the range of 300–600 mm and 1.3–2 bara, respectively. The project's objectives are as follows:

1) To assess the methodology proposed by Melguizo-Gavilanes et.al. [1] against available experimental data, and evaluate its predictive capabilities.
2) To improve the deflagration model by conducting a sensitivity analysis to evaluate key influencing parameters.
3) To develop an alternative approach that relates release conditions (i.e., vent diameter and release pressure) via the Reynolds number to the visible flame speed, using existing experimental data.
4) To validate the updated methodology and evaluate its performance using the same set of experimental data as in Objective 1.

As the goal of this study is to develop a more reliable model that yields more accurate overpressure estimates resulting from hydrogen venting. We aim to visualise the research outcomes in ways— such as heat maps— that provides valuable and practical insights for practitioners at hydrogen facilities of any scale. For instance, the outputs including expected overpressure, released hydrogen mass, mass flow rate, dispersion profile will be plotted against the vent release conditions such as vent diameters and vent release pressures to effectively present the prediction output. These visualisations are intended to enable a quick assessment of parameters, such as released hydrogen mass, mass flow rate, plume size, and resulting overpressure, based on known release conditions (i.e., vent diameter and release pressure). Ultimately, this will help ensure that potential catastrophic events in hydrogen facilities are adequately anticipated and prevented.

4 Methodology

The methodology for overpressure assessment for hydrogen venting scenarios, i.e., the delayed ignition of unconfined and uncongested vertical hydrogen jet release, is introduced herein by continuing the work from Melguizo-Gavilanes et.al. [1]. The approach was structured as a two-step procedure, as shown in Figure 4: (i) dispersion modelling and (ii) overpressure modelling. Dispersion model estimates hydrogen dispersion under various venting conditions using a standard consequence modelling software. The latter step involves computation of blast loads based on the dispersion outcomes, by revisiting the work of Dorofeev [17].

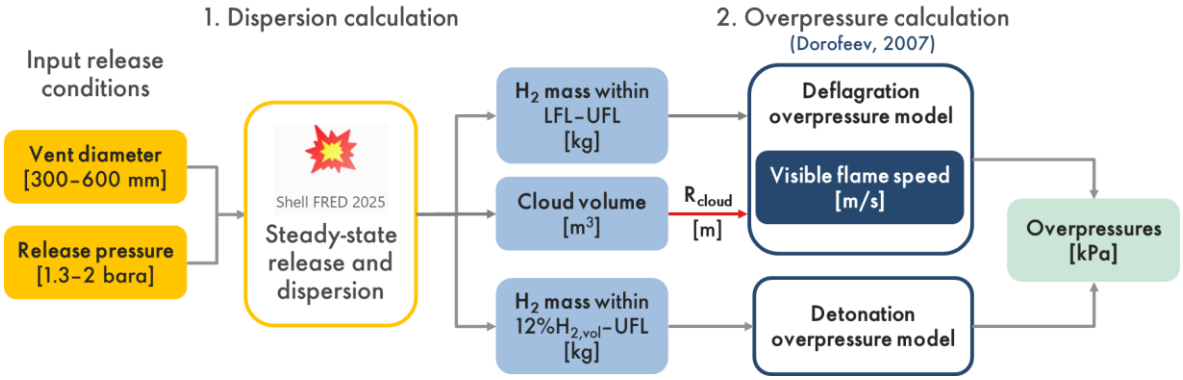

Figure 4 Schematic of workflow based on the methodology of Melguizo-Gavilanes et.al. [1]

4.1 Dispersion modelling

The dispersion model provides an estimate of the dispersed flammable cloud from given release conditions such as vent geometries, venting conditions, and external environment. Dispersion simulations are performed using the consequence modelling software Shell FRED (Fire Release Explosion Dispersion), which offer adequate first-order approximations of dispersion footprints. This tool has been continuously improved and extensively validated with large-scale experiments. FRED provides information such as hydrogen mass contained within the cloud and cloud volume (for estimation of effective cloud radius), which are key input values for the estimation of the deflagration and detonation overpressures in the subsequent steps. Steady-state gas releases were assumed in the present methodology, meaning the mass flow rate of gas is constant.

The modelling approach used for predicting steady-state release of gas from a pressurised source is briefly described below. The formation and behaviour of the gas plume was simulated under varying vent dimensions and pressures using FRED [26].

4.1.1 Steady-state gas/vapour release model

Hydrogen venting scenario is computed using pressurised release model, in which FRED [26] requires either gas source pressure or mass flow rate as an input. This allows for the calculation of other independent sub-models, one of which is the dispersion model, to be discussed further in Section 4.1.2.

Steady-state release conditions can be classified as sonic and subsonic flows. The selection of the proper expression for calculation of mass flow rate or source pressure (Equation 9 and Equation 10) depends on whether the pressure ratio of the release $(\frac{P}{P_{gas}})$ is greater or lesser than the critical pressure ratio (P_c) (see Equation 8).

$$P_c = \left(\frac{2}{\gamma+1}\right)^{\frac{\gamma}{\gamma-1}} \quad \textit{Equation 8}$$

$$\frac{P}{P_{gas}} < P_c;\ \dot{m}_{sonic} = \frac{C_d * A * P_{gas}}{\sqrt{\frac{8314}{MW} * T_g}} * \sqrt{\gamma * \left(\frac{2}{\gamma+1}\right)^{\frac{\gamma+1}{\gamma-1}}} \quad \textit{Equation 9}$$

$$Otherwise;\ \dot{m}_{subsonic} = \frac{C_d * A * \psi_0 * P_{gas}}{\sqrt{\frac{8314}{MW} * T_g}} * \sqrt{\gamma * \left(\frac{2}{\gamma+1}\right)^{\frac{\gamma+1}{\gamma-1}}} \quad \textit{Equation 10}$$

$$\psi_0 = \left(\frac{P}{P_{gas}}\right)^{\frac{1}{\gamma}} * \sqrt{1 - \left(\frac{P}{P_{gas}}\right)^{\frac{\gamma-1}{\gamma}}} * \sqrt{\left(\frac{2}{\gamma-1}\right) * \left(\frac{\gamma+1}{2}\right)^{\frac{\gamma+1}{\gamma-1}}} \quad \textit{Equation 11}$$

Where $\gamma = c_p/c_v$ is the isentropic expansion factor. $\dot{m}$ is mass flow rate (kg/s) according to either sonic or subsonic flow. C_d is discharge coefficient (~0.8 for gases). A is defined as hole area (m^2). MW is gas molecular weight (kg/kmol). T_g is vessel temperature (K). P_{gas} is gas absolute pressure (Pa). P is ambient pressure (Pa).

4.1.2 Jet dispersion model

Hydrogen jet dispersion is modelled using AEROPLUME [27], which is suitable for gaseous jets releases. The model allows for releases in various directions and can describe the dispersion of both buoyant and dense gases. In addition, AEROPLUME provides accurate dispersion estimates in close proximity, up to 1000 m from the source, which is sufficient to capture cloud sizes typically ranging from 20 to 30 m downwind, based on the scope of the considered release conditions. The contour profiles displayed in FRED are generated using the standard Gaussian model. Figure 5 represents examples of Gaussian dispersion contours for various plume sizes at lower flammability limit (LFL), resulting from different release conditions.

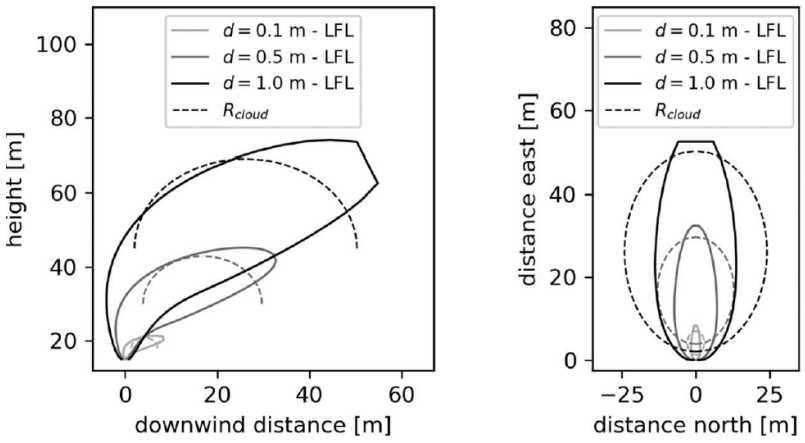

Figure 5 Side (left) and top (right) views of dispersed clouds. Gaussian dispersion contours (black solid line) of the entire hydrogen cloud at 4%vol H_2/air or its LFL based on different release conditions. Hemispherical clouds (dash lines) containing same volume of hydrogen cloud. [1]

The Gaussian dispersion model can provide the concentration profiles within the plume. The near-field expression (up to 1000 m) [26] to determine concentration at a point (x, y, z) downwind of a release source located at a coordinate (0,0, h) is given as:

$$C(x,y,z) = \frac{\dot{m}}{2\pi u \sigma_y \sigma_z} e^{\frac{-y^2}{2{\sigma_y}^2}} \left(e^{\frac{-(z-h)^2}{2{\sigma_z}^2}} + e^{\frac{-(z+h)^2}{2{\sigma_z}^2}} \right) \quad \textit{Equation 12}$$

Where $\dot{m}$ is source mass flow rate (kg/s). u is wind velocity (m/s). h is a release height/plume centreline (m). z is height above grade (m). y is lateral displacement from plume centreline (m). σ_y and σ_z are lateral and horizontal dispersion parameters obtained from field tests, which are influenced by distance, environmental conditions (classified by Pasquill-Gifford stability classes [28]), surface roughness, and dispersion time average.

Typically, the dispersed cloud profile exhibits a complex geometry (see Figure 1), with a non-uniform hydrogen concentration within the cloud. A simplified assumption is made where a cloud is modelled as a hemisphere containing a same volume of gas within the concentration contour, showed in Figure 5. The dashes lines depict the cloud contour of the equivalent-volume hemispheres. From the side view, the hemispherical approximation underestimates the plume width, while from the top view, it overestimates the cloud spread. This overestimation in one direction appears to compensate for the underestimation in the other, demonstrating that hemisphere provides a sufficient representation of the actual cloud.

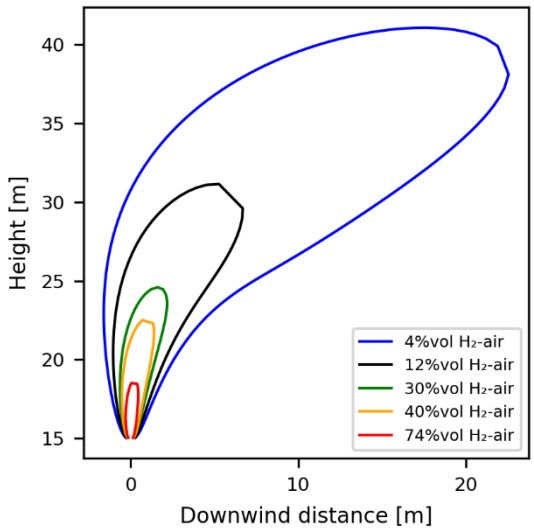

Figure 6 Side-view dispersion contours simulated by FRED at concentrations of 4%, 12%, 30%, 40%, and 74%vol H_2/air. The initial release condition: $d = 300\ mm$ and $P_{source} = 2\ bara$.

An additional point to consider is where within the cloud hydrogen could potentially ignite to generate the combustion regimes of interest— deflagration and detonation. In reality, hydrogen clouds are non-uniform, with concentration contours varying at different locations within the cloud. Typically, the most reactive region of the hydrogen cloud locates around stoichiometric concentration, approximately 30% (300000 ppm contour line) to 40%vol H_2/air (400000 ppm contour line), which is found to be relatively close to the release point (see Figure 6).

4.1.3 FRED scenario configuration

The "Pressurized Release" scenario was chosen to simulate pure hydrogen gas venting through circular openings. This study primarily focuses on the variation of two release parameters: (i) vent diameters and (ii) vent release pressures.

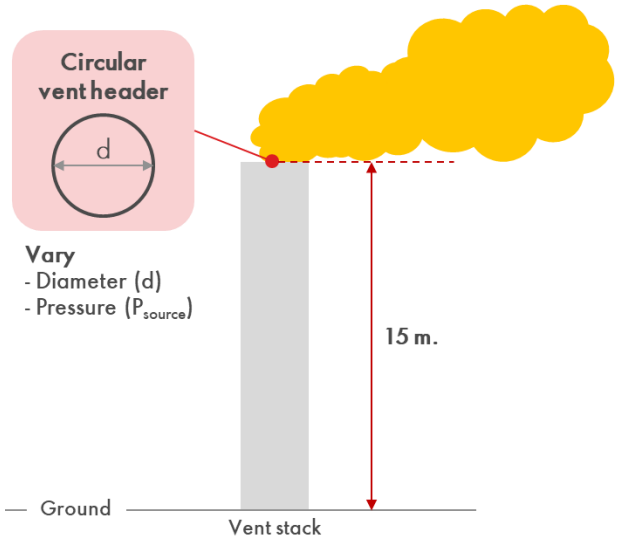

Figure 7 Schematic of the venting configuration considered in this study.

Based on the information from a Shell's facility, the hydrogen is vented through a main vent header, see Figure 7. The release is at 40°C upward to open atmosphere in vertical direction at the height of 15 m above grade. Table 2 indicates the meteorological conditions that are considered in this study.

Table 2 Meteorological conditions

Ambient temperature	15°C
Relative humidity	70%
Wind speed	5 m/s
Wind direction	Northerly wind
Atmospheric pressure	1.01325 bara
Stability class	D-Neutral

The choice of dispersion contour is crucial as it determines the hydrogen mass contributing to the blast. This value serves as an important input for estimating overpressure effects of deflagration and detonation waves in the latter analyses. Both are two distinct combustion regimes having different underlying combustion physics. Thus, the boundaries of consideration—namely the flammability and detonability limits—differs.

The approach is to define concentration contour limits for non-uniform concentration clouds, which serve to bound the amount of hydrogen gas contributing to the blast loads under each combustion regime of interest. The flammability limit lies between 4% and 74%vol H_2/air for deflagration regime (see contour lines in Figure 6). In contrast, the detonability limit differs, as it is not a fixed value of concentration. Instead, it depends on ratio of the length scale determined by system geometry to detonation cell size (i.e., characteristic length scale in detonation) [29]. As it is explained by combustion physics based on tube experiments reported in the database [30], the lower detonability limit can be identified around the concentration where the detonation cell size increases sharply, which is found between 14%vol and 13%vol H_2/air. Therefore, the lower threshold of 12%vol H_2/air is taken as the onset of detonability, with the upper limit extending to 74%vol H_2/air (see contour lines in Figure 6).

4.2 Overpressure modelling

Once the dispersion of gas clouds is computed, the next step is to calculate the overpressures. The adopted approach here builds upon the work of Melguizo-Gavilanes et.al. [1], which revisits the work of Dorofeev [17] for estimating unconfined and uncongested deflagration and detonation overpressures.

4.2.1 Unconfined detonation model

Equation 13 [17] is proposed for overpressure estimates of a blast wave resulting from vapor cloud detonation in the open air. The model solely influenced by the mass of hydrogen within the cloud contour, which is embedded in the term R^*.

$$P_1^* = \frac{0.34}{R^{*4/3}} + \frac{0.062}{R^{*2}} + \frac{0.0033}{R^{*3}} \qquad \textit{Equation 13}$$

Which is valid for $0.21 < R^* < 3.77$

$$P^* = \frac{\Delta p}{p_0} \qquad \textit{Equation 14}$$

$$R^* = R\left(\frac{p_0}{E}\right)^{1/3} \qquad \textit{Equation 15}$$

The dimensionless variables so-called Sachs variables, P^* and R^*, are a scaled overpressure and scaled distance, in which $\Delta p = p - p_0$ is the overpressure (kPa), where p is the pressure at the point of interest (kPa) and p_0 is atmospheric pressure (kPa). R refers to the distance or radii from the blast epicentre (m), and E represents anticipated combustion energy released (J), which is influenced by the associated amount of H_2 mass present in the cloud (kg) and lower heating value (LHV), taken as 120 MJ/kg.

4.2.2 Unconfined deflagration model

In the case of delayed ignition following the release of a flammable cloud, the pressure generated during deflagration is attributed to the expansion of burned gases and the pushing of the gas ahead of the flame. Consequently, estimating deflagration overpressure takes into account the visible flame speed, as follows [17]:

$$P_2^* = \left(\frac{V_f}{a_0}\right)^2 \frac{\sigma - 1}{\sigma}\left(\frac{0.83}{R^*} - \frac{0.14}{R^{*2}}\right) \qquad \textit{Equation 16}$$

which is valid for $0.21 < R^* < 3.77$ and $V_f \leq 500\ m/s$.

Where the description of the Sach variables P^* and R^* remained the same. V_f represents the visible flame speed (m/s), or in other words, flame speed in the laboratory frame of reference. a_0 is speed of sound in air, taken as a constant value of 353 m/s at 300 K. σ denotes the expansion ratio (i.e., the ratio of density of unburnt gas to that of the burnt gas).

Equation 16 requires only a single value of flame speed, V_f. However, in reality, for a given set of initial and boundary conditions, V_f varies depending on the location of interest within the cloud, introducing further complexity in estimating deflagration overpressure. A simpler approach is through the approximation of flame speed V_f as a function of distance from the ignition centre and

the fundamental combustion properties (FCP), such as expansion ratio σ, laminar burning velocity S_L and flame thickness δ, for freely propagating flames, as described in Equation 17 [17].

$$V_f = A\sigma(\sigma - 1)S_L\left(\frac{R}{\delta}\right)^{\frac{1}{3}} \qquad \textit{Equation 17}$$

Where $A = 8.5 \times 10^{-3}$ is obtained by fitting experimental data over a wide range of fuel-air mixtures to the expression above using least-squares regression. R is distance from the ignition centre (m). S_L is the laminar burning velocity (m/s). δ represents flame thickness (m). The FCP depend on fuel concentration and are not a unique value, as shown in Figure 8.

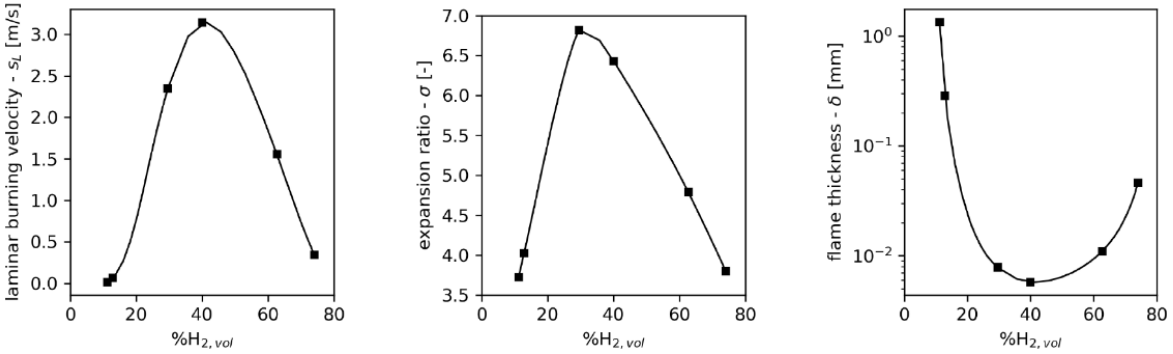

Figure 8 S_L, σ, and δ as functions of hydrogen concentrations in air (%vol). Markers are shown for 11.2, 12.8, 19.6, 40.1, 62.7, and 74%vol H_2/air for initial conditions of 100 kPa and 300 K [1].

Real gas release scenarios form non-uniform clouds, and if the cloud is ignited after a delay, flames are generated. The speed at which the flame propagates varies across different locations within the cloud. However, the deflagration model requires a single representative visible flame speed, denoted as V_f. To determine V_f for a given release, a single value for each FCP is required, which depends on the hydrogen gas concentration. Various methods can be used to obtain FCP values [1]. One approach involves calculating average FCP values by integrating over the cloud volume, accounting for the influence of hydrogen concentration, and applying simplifying assumptions[1]. An alternative method is to use CFD simulations; however, this is not preferred in this study due to the impracticality of applying CFD at the industrial scale of interest, given the extensive computational time and spatial resolution required. Therefore, an arithmetic average of FCP values is taken over the hydrogen concentration range from 29.6% vol H_2/air to the upper threshold of 74% vol H_2/air, as this is deemed to provide a good approximation of the visible flame speed [1]. The resulting average FCP values are: $S_L = 1.847$ m/s, $\sigma = 5.46$, and $\delta = 1.76 \times 10^{-5} m$.

In addition to FCP considerations, the visible flame speed must account for a distance R. Therefore, a further simplification is made by computing the flame speed at the distance from the ignition centre to the edge of the hemispherical cloud (see dash lines in Figure 5)—referred to effective or equivalent cloud radius (R_{cloud}). This R_{cloud} is based on the assumption of an equivalent hemisphere containing the same volume of gas as the dispersed cloud and can be estimated using Equation 18.

$$R_{cloud} = \left(\frac{3}{2\pi}V_{cloud}\right)^{\frac{1}{3}} \qquad \textit{Equation 18}$$

Where V_{cloud} is the volume of gas cloud within the flammability limit (m^3). R_{cloud} is effective cloud radius (m).

[1] *A hydrogen cloud assumes to be a hemisphere having non-uniform concentration with its maximum concentration is at the cloud centre and then decreasing linearly towards the edge.*

To summarise, the methodology implemented herein for overpressure predictions from the work of Melguizo-Gavilanes et.al. [1] can be divided into two stages: modelling the hydrogen dispersed cloud and evaluation of overpressure, respectively, based on defined pairs of vent diameters and vent release pressures. The dispersion model provides information on the mass of hydrogen gas in the cloud and the cloud volume, following the flammability and detonability limits. This information is a crucial input for the computation of overpressures, through the deflagration and detonation correlations of Dorofeev S. [17]The next section provides an example to illustrate the result of the model for better understanding on how deflagration and detonation models works.

5 Scenario configuration and results

This section provides an example of hydrogen venting that demonstrates the outcome of the methodology, including results from both deflagration and detonation models, as well as their physical significance. A vent diameter of 300 mm and a vent pressure of 2 bara are selected for illustration. The release is at 15 m following the configuration in Section 4.1.3.

As the methodology comprises two stages, the first involves dispersion calculations using FRED for the given hydrogen venting conditions (d = 300 mm and P_{source} = 2 bara). The volume and mass of hydrogen can then be determined based on the flammability and detonability limits. Subsequently, deflagration and detonation estimates can be obtained using the correlations described in the previous section, which will be elaborated on in more detail below.

5.1 Unconfined detonation model

Figure 9 illustrates a detonation scenario following delayed ignition of a hydrogen cloud. Under typical industrial conditions, it is generally rare for detonation to be initiated directly, as the energy present is usually insufficient to trigger detonation of the flammable cloud. A more plausible pathway involves flame acceleration, leading to a transition from deflagration to detonation. However, this combined phenomenon remains unlikely in the present case, as the release is unconfined and uncongested. In practice, congestion and confinement significantly enhance flame acceleration, but these factors are absent in the scenario considered [22,23].

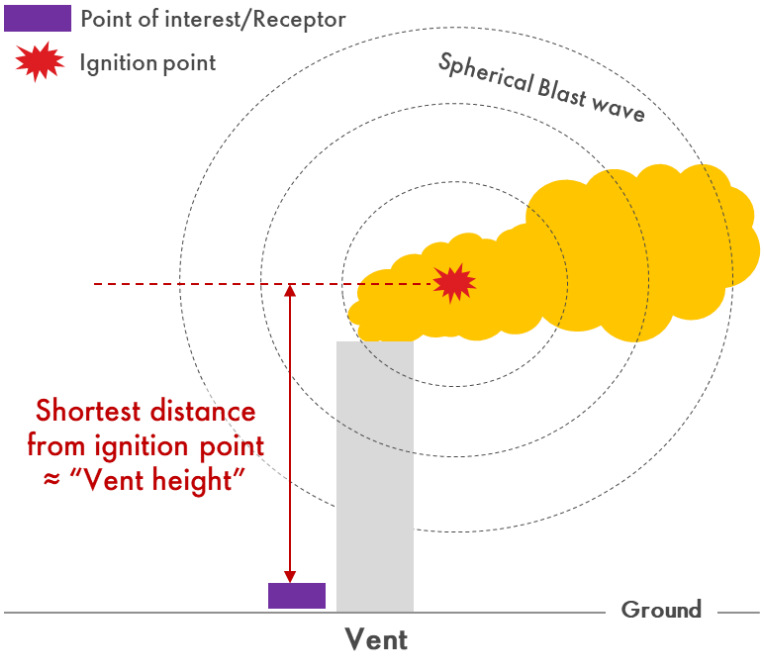

Figure 9 Schematic of hydrogen detonation scenario. The yellow cloud illustrates dispersed hydrogen from a vent header. The dashed circles represent generated blast waves after detonated reactive gas mixture. The ignition location is assumed to be at around stoichiometric concentration H_2/air (30-40%vol), where the gas mixture is most reactive.

Therefore, while detonation has been found to be unlikely [7], it cannot be entirely ruled out. To maintain a conservative approach, this study assumes that detonation could be initiated in the most reactive region of the cloud—around the stoichiometric hydrogen–air mixture. The potential overpressures generated are attributed to spherical blast waves, represented by dashed lines in Figure 9.

Figure 10 illustrates the detonation overpressure profile (obtained from Equation 13) as a function of distance from the ignition source, plotted on a logarithmic scale. The resulting curve is based on the release condition of a vent diameter of 300 mm and source pressure of 2 bara, provided for representative purpose. Dispersion model provides the mass of hydrogen within the detonability limit as 3.06 kg. Detonation correlation estimates the maximum blast load at the ignition point, although this value is extremely conservative.

Since the detonation correlation overestimates the magnitude of blast waves near the ignition point—given its validity range of $0.21 < R^* < 3.77$—the model provides reliable detonation overpressure estimates at distances from the ignition source corresponding to $3.2 < R < 57.9$ m. A more meaningful value to report as the maximum threshold for a given release condition is the overpressure at the shortest distance between the ignition source and ground level—approximately the vent height (15 m for the current configuration)—where personnel and facility may be present, see Figure 9. Hence, the potential detonation overpressure resulting from hydrogen venting release condition of $d = 300\ mm$ and $P_{source} = 2\ bara$ is 42.5 kPa (at 15 m from ignition point), located on ground next to the vent stack.

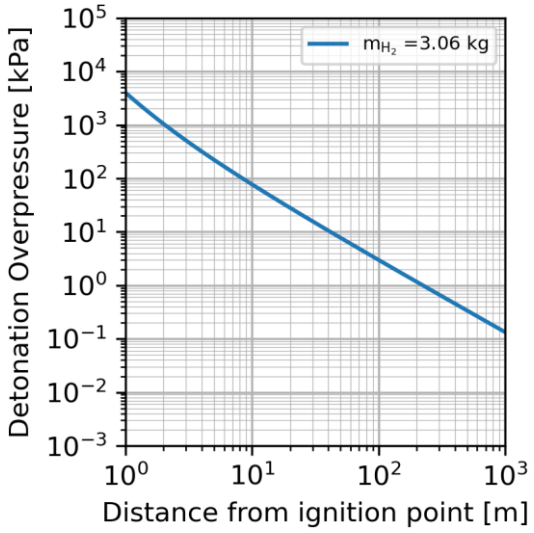

Figure 10 Detonation profile for vertical hydrogen release having the release condition of $d = 300\ mm$ *and* $P_{source} = 2\ bara$.

5.2 Unconfined deflagration model

Figure 11 illustrates a deflagration scheme following delayed ignition of a hydrogen cloud. The overpressure generated results from the expansion of burned gases and the pushing of the unburnt gas ahead of the flame. Consequently, deflagration overpressure influences by how rapidly the flame propagates—determined by a parameter namely visible flame speed. Due to the non-uniform and complex geometry of the dispersed cloud, evaluating the visible flame speed is challenging, as it depends on local hydrogen–air concentrations. A simplification is made for the cloud, assumed to be hemispherical, containing the same volume of gas mixture as the dispersed cloud.

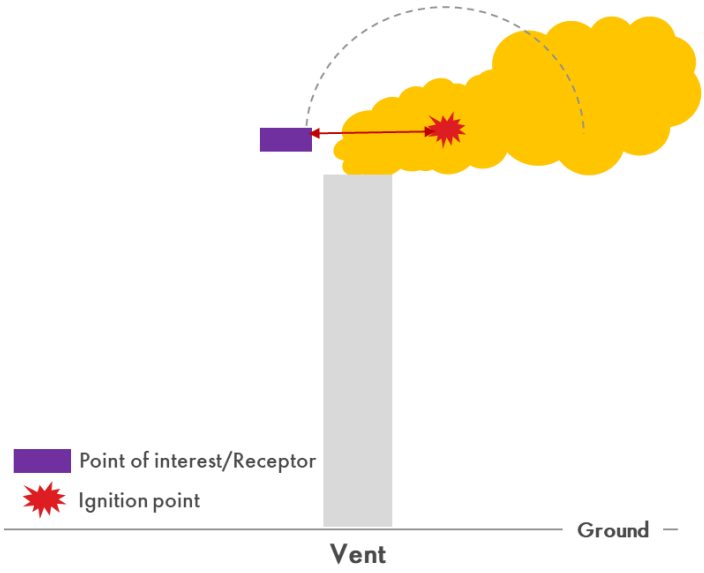

Figure 11 Schematic of hydrogen deflagration scenario. The yellow cloud illustrates dispersed hydrogen from a vent head. The dashed semi-circle represents an equivalent hemisphere containing the same volume of gas as the yellow cloud. Ignition location is assumed to be at around stoichiometric concentration of H_2/air (30-40%vol), where the gas mixture is most reactive.

The dispersion model estimates the cloud volume and hydrogen mass within the detonability limits as 1922.9 m³ and 11.88 kg, respectively. Figure 12 represents an example of the predicted deflagration overpressure profile (obtained from Equation 16) as a function of distance from the ignition source, based on the same release conditions discussed in the previous section. Given the model's validity range of $0.21 < R^* < 3.77$, it provides reliable deflagration overpressure estimates at distances from the ignition source corresponding to $5.1 < R < 91.0$ m for release condition of $d = 300\ mm$ and $P_{source} = 2\ bara$.

Unlike detonation regime, deflagration produces a peak overpressure at a certain distance from the ignition source (see Figure 12), which is expected to locate at the cloud edge. According to the overpressure profile in Figure 12, the peak (read as 0.8 kPa) appears at 8 m, corresponding to the distance from the ignition source (marked in red in Figure 11) to the cloud edge (dashed semi-circle in Figure 11). Calculation based on the hemisphere cloud (Equation 18) yielded the equivalent radius of 9.7 m, which closely aligns with the peak location in Figure 12. The visible flame speed velocity at cloud edge, calculated using Equation 17, is 31.34 m/s, contributing to the peak deflagration overpressure.

Beyond the peak, overpressures then decay accordingly as the point of interest (purple box in Figure 11) moves further away from the ignition source, beyond the cloud boundary. The behaviour can be physically explained by the fact that flame propagation and acceleration occur only within the flammable mixtures. This means the flame continues to accelerate up to the cloud edge, where combustible gas is still present, and ceases to accelerate beyond the boundary. As such, the maximum flame speed is typically reached at the cloud edge, which consequentially contributes to the generation of peak overpressure.

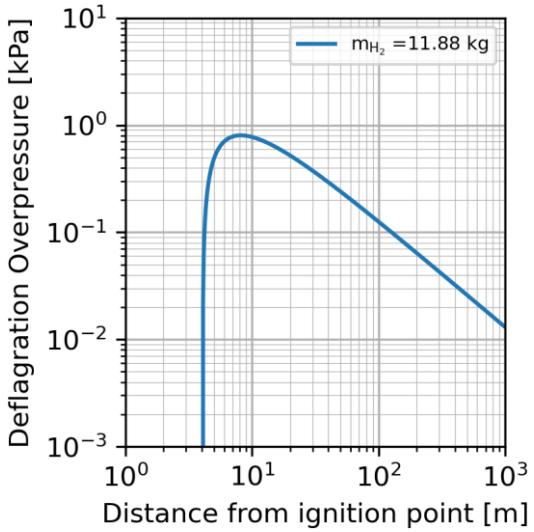

Figure 12 Deflagration profile for vertical hydrogen release having the release condition of $d = 300\ mm$ *and* $P_{source} = 2\ bara$.

6 Overpressure model performance

The predicted overpressure obtained from the proposed methodology of Melguizo-Gavilanes et.al. [1] is tested against reported overpressure from available experiments. Initially, it was a significant challenge to source relevant experiments to validate the model, as limited information was reported, particularly large releases of hydrogen into open air in vertical direction. Only one experiment matched the vertical release scheme, while others involving horizontal releases were excluded from this validation. Fortunately, a conference paper by Air Products became available in late April 2025 during the course of this study, containing valuable information on open-air vertical hydrogen releases. These additional experiments will also be tested and included in the later part of this section.

6.1 Validation with a vertical large-scale test

The methodology was previously tested against the experiment by Schneider and Pförtner [31], which involved quiescent hydrogen-air deflagration of a hemispherical cloud with a radius of 10 m containing a uniform hydrogen concentration of 29.7% in air (c.a. 51 kg of hydrogen). The prediction showed good agreement with the reported experimental data; however, this approach has not yet been tested against jet release scenarios having non-uniform concentrations.

An experiment conducted by the team of Groethe et.al. [7] reported a vertical hydrogen jet release through a nozzle with a diameter of 42 mm and source pressure of 24 bar. The peak overpressure reported was 4 kPa, located at approximately 7 m from the point of ignition.

Knowing the release diameter and the source pressure, the estimation of hydrogen mass and cloud volume within the contour limits (i.e., 4-74%vol H_2/air for deflagration and 12-74%vol H_2/air for detonation) can be obtained through FRED. The visible flame speed can be evaluated based on the effective cloud radius using Equation 17 with the assumption of a hemisphere containing the same gas volume as the dispersed cloud. Subsequently, deflagration and detonation overpressures can be computed at the same distance as reported in the experiment. Relevant results are summarised in Table 3 and the overpressure-distance profiles for deflagration (Figure 13) and detonation (Figure 14) are provided herein.

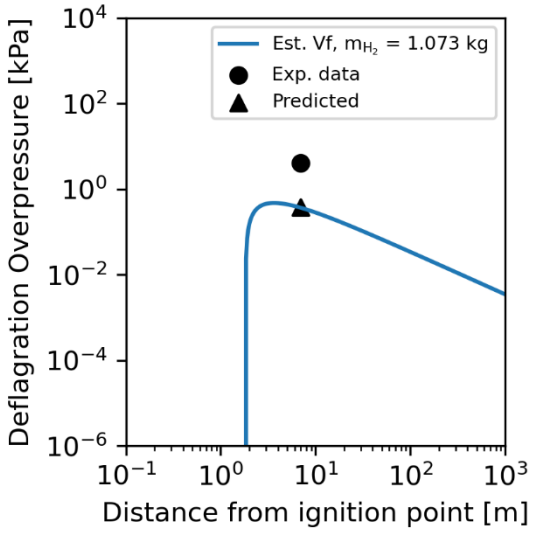

Figure 13 Deflagration overpressure-distance profile for $d = 42\ mm$ and $P_{source} = 24\ bar$ in blue. A circle and triangle markers represent experimental data and predicted value, respectively.

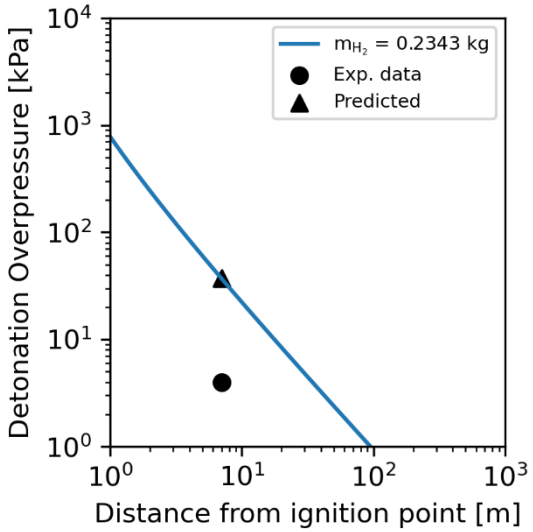

Figure 14 Detonation overpressure-distance profile for $d = 42\ mm$ and $P_{source} = 24\ bar$ in blue. A circle and triangle markers represent experimental data and predicted value, respectively.

Table 3 Summary of validation results for Groethe M. et.al. [7] experiment.

Case	d (mm)	P_{source} (bara)	m_{H_2} within contour (kg)	V_{cloud} within contour (m^3)	R_{cloud} (m)	$V_{f,R_{cloud}}$ (m/s)	R (m)	Predicted overpressure P^*P_0 (kPa)
Deflagration	42	24	1.073	179.4	4.4	24.1	7	0.37
Detonation	42	24	0.2343	-	-	-	7	37.08

The peak overpressure reported by Groethe et.al. [7] is 4 kPa. The deflagration correlation underestimates the blast load by a factor of 10.8, whereas the detonation model overpredicts the blast overpressure by a factor of 9.3. This wide prediction gap—where deflagration and detonation overpressures serve as the lower and upper bounds for a given vent diameter and pressure—stresses a need for improvement to achieve a more reliable estimation model.

6.2 Validation against the Air Products experiments

Air Products carried out more than 20 open-air experiments on the delayed ignition of vertical hydrogen releases. The release nozzle diameters ranged from 50.8 mm (2 inch) to 203.2 mm (8 inch), and the hydrogen mass flow rates varied from 0.15 kg/s to 0.57 kg/s, both of which are important inputs to the dispersion model. FRED enabled calculation of the source pressures, which corresponds to a range of 1.01 bara to 4.71 bara depending on input conditions. Table 4 summarises the chosen set of experiments performed by Air Products [32].

Some tests have similar release diameters and mass flow rates; however, minor differences, such as release temperatures, ignition delays and environmental factors including ambient temperature and wind speed, affecting the evaluation of available hydrogen mass within the concentration contour, eventually influencing the resulting overpressure. Most reported parameters were incorporated into FRED to closely reproduce results with the experiment setup. Only the ignition delay time was omitted in this analysis, as currently the mass calculation is limited to steady-state dispersion, not time-defined dispersion.

Table 4 Summary of vertical release conditions for selected Air Products tests

Release conditions	Test code	d (mm)	$\dot{m}_{H_2}$ (kg/s)	P_{source} (bara)	Calculated exit Mach No.	Ignition delay (s)	Wind speed at 10 m height (m/s)
Warm releases (−27℃ to 6 ℃)	A05	101.6	0.15	1.04	0.2	6	3.6
	A07	101.6	0.25	1.01	0.3	3	6.7
	A09	101.6	0.46	1.3	0.5	3	8.5
	A10	101.6	0.49	1.35	0.5	3	2.1
	A12	50.8	0.46	4.71	0.8	3	3.0
	A14	203.2	0.49	1.03	0.1	3	1.5
Cold releases (−158℃ to −83 ℃)	B06	203.2	0.47	1.03	0.1	3	1.0
	B07	50.8	0.57	4.56	0.8	3	2.6
	B10	50.8	0.55	4.63	0.8	3	1.6
	B11	76.2	0.56	1.96	0.7	3	1.6
	B12	76.2	0.52	1.92	0.7	3	3.7
	B13	76.2	0.53	2.00	0.7	6	2.6
	B14	76.2	0.52	1.94	0.7	8	1.6
	B15	76.2	0.5	1.82	0.7	11	2.1

The outcomes from FRED, including hydrogen mass and cloud volume under deflagration and detonation contour limits, are used to compute overpressures. Results are summarised in the Appendix A1.

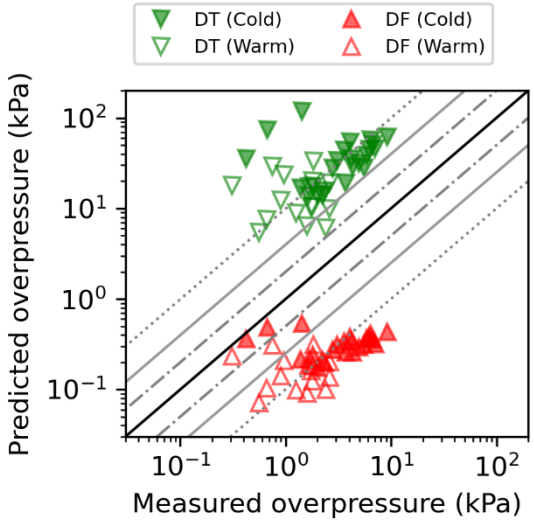

Figure 15 Model performance shown on a log-log scale plot of predicted blast overpressure using the methodology of Melguizo-Gavilanes et.al. [1] against the reported overpressure from Air Products, based on two different release temperatures. Filled and unfilled markers denote cold and warm release experiments, respectively. Red triangles represent overpressure estimates from the deflagration (DF) model. Green downward triangles indicate overpressure estimates from the detonation (DT) model. Solid black line denotes a perfect match between predicted and experimental overpressures. Grey dash-dot lines represent a factor of two overestimation and underestimation relative to the reported overpressures. Solid grey lines are guided lines

of four-fold overestimation and underestimation. Grey dashed lines serve as an indicator of an order magnitude of overestimation and underestimation.

Figure 15 shows the predicted overpressures from deflagration (denoted as DF in red markers) and detonation (labelled as DT in green markers) correlations, plotted against actual measurements from experiments. The predictive capabilities for deflagration and detonation models were categorised into four over/underestimation prediction bands (each including the upper bound): (i) >10, (ii) between 4 and 10, (iii) between 2 and 4, and (iv) between 1 and 2, where a factor of one indicates a perfect prediction (i.e., predicted overpressure equals measured overpressure), as listed in Table 5.

Table 5 Summary of deflagration and detonation model performance with Air Products experiments. The table lists the number of points falling within each range of over/underprediction factors. The bold number in each prediction band indicates that the interval includes that upper limit.

Prediction bands	**Total 40 data points**	
	Detonation	**Deflagration**
>10x	16 (40%)	24 (60%)
4x–**10x**	22 (55%)	11 (27.5%)
2x–**4x**	2 (5%)	2 (5%)
1x–**2x**	0	3 (7.5%)

Out of 40 data points, the deflagration model consistently underpredicts overpressure (DF, red markers in Figure 15), with the majority—60% of all estimates—being underpredicted by more than a factor of 10. This is followed by 27.5% of predictions falling within a factor of 4 to 10, 5% within a factor of 2 to 4, and 7.5% within a factor of 2. The detonation model, on the other hand, yields highly conservative results (DT, green markers in Figure 15). Of the 40 predictions, 95% exceed a factor of 4, and 40% exceed a factor of 10. These results highlight the need for an improved methodology to reliably estimate overpressures.

7 Dispersion and overpressure heat maps results

The following sections present heat map results based on the methodology of Melguizo-Gavilanes et.al. [1] including outcomes from both dispersion and overpressure models, for the process venting conditions within the range of $d = 300 - 600$ mm and $P_{source} = 1.3 - 2$ bara. The design allows for releases through a header located 15 m above ground. The surrounding conditions were fixed as described in Section 4.1.3 (FRED scenario configuration). A total of 64 FRED simulations were conducted, generating dispersion parametric spaces that serve as inputs for overpressure calculation in the subsequent stages.

7.1 Dispersion results

The selected metrics obtained from FRED are summarised in the heat maps shown in Figure 16. These include vent mass flow rate, hydrogen mass within flammability limit [LFL–UFL] relevant for deflagration and detonability limit [12% vol H_2/air–UFL] relevant for detonation, which are essential for estimating the released combustion energy, E, used in overpressure quantification.

Given the hydrogen vent header with diameters of 300–600 mm and release pressure of 1.3–2 bara, the resulting hydrogen mass flow rate ranges from 3.8–27.3 kg/s, with H_2 mass of 6.6–85.1 kg within the flammability limit and 1.8–23.1 kg within detonability limit.

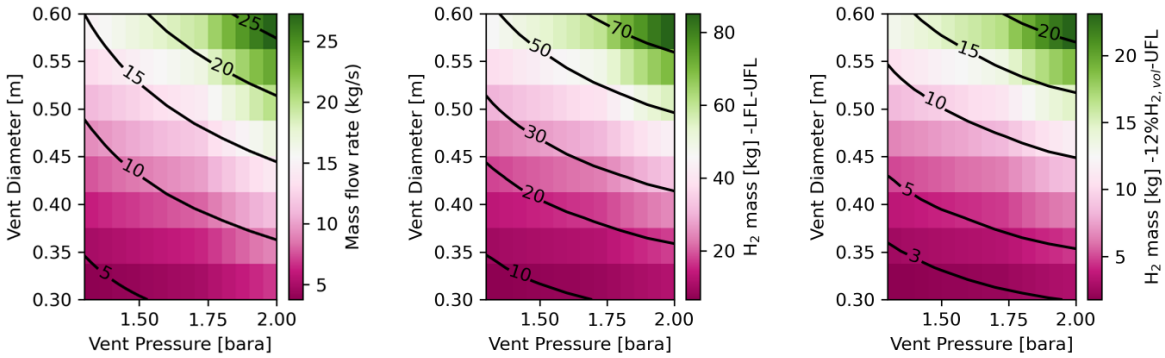

Figure 16 Dispersion results obtained from FRED for the process venting conditions within the range of $d = 300 - 600\ mm$ *and* $P_{source} = 1.3 - 2\ bara$*. Heat maps (from left to right) include (i) hydrogen mass flow rate (kg/s), (ii)* H_2 *mass within the flammability limits (kg), and (iii)* H_2 *mass within the detonability limits (kg).*

The heat map enables efficient visualisation of a metric of interest corresponding to variations in vent diameters and pressures, serving as a guide for vent designs or consequence assessments under given constraints. The black solid lines represent constant values of the metric of interest for specific combinations of vent pressures and vent diameters. This becomes particularly useful in practical scenarios — for example, if a vent is limited to releasing below 15 kg/s, what could the possible vent designs be? Referring to the first heat map on the left of Figure 16, by following the black contour line corresponding to 15 kg/s, a valid design would allow vent diameters between 450–600 mm and release pressures between 2–1.3 bara. One possible selection could be a 600 mm vent diameter paired with a 1.3-bara release pressure.

7.2 Overpressure results

7.2.1 Unconfined detonation

To report the estimated detonation overpressure, the location of interest is chosen at a distance of 15 m from the ignition point—i.e., equivalent to the vent height—representing a maximum overpressure at the minimum distance that could potentially affect personnel and equipment located beneath a vent stack. At greater distances, overpressures are expected to decay. Detonation overpressure can be simply computed using the hydrogen mass estimated from FRED, based on the detonability limit (12% vol H_2/air – UFL), using Equation 13. Although detonation is unlikely under conditions without confinement or congestion, it is still advisable to retain this conservative estimate as an upper limit. The detonation overpressure results within the parametric space are presented as a heat map in Figure 17, with predicted values ranging from 32.6 to 115.5 kPa. An increase in overpressure is observed to correlate with an increase in hydrogen mass within the detonability limit.

The resulting overpressure values correspond to a range of destructive outcomes. At 32.6 kPa, near-complete destruction of houses and the toppling of large trees can be expected. At higher levels (115.5 kPa), severe injuries or fatalities are likely for occupants of unstrengthened buildings due to direct blast effects, building collapse, or translation [33].

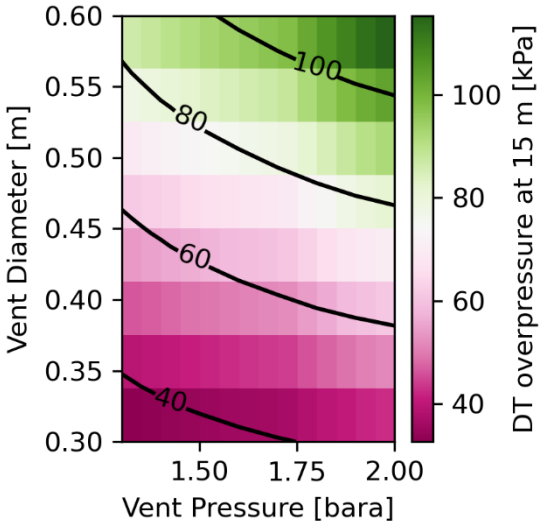

Figure 17 Heat map showing detonation overpressure estimates at 15 m from the ignition source for combinations of release conditions within the range of $d = 300 - 600\ mm$ *and* $P_{source} = 1.3 - 2\ bara$.

7.2.2 Unconfined deflagration

Computing deflagration overpressures (Equation 16) indeed requires the visible flame speed. Using dispersion results, the effective cloud radius can be calculated from Equation 18, based on the assumption of a hemispherical cloud. This, in turn, enables the estimation of visible flame speed via Equation 17. The equivalent cloud radius was found to range from 8 to 19 m, corresponding to visible flame speed estimates of approximately 29 to 39 m/s, as shown in Figure 18.

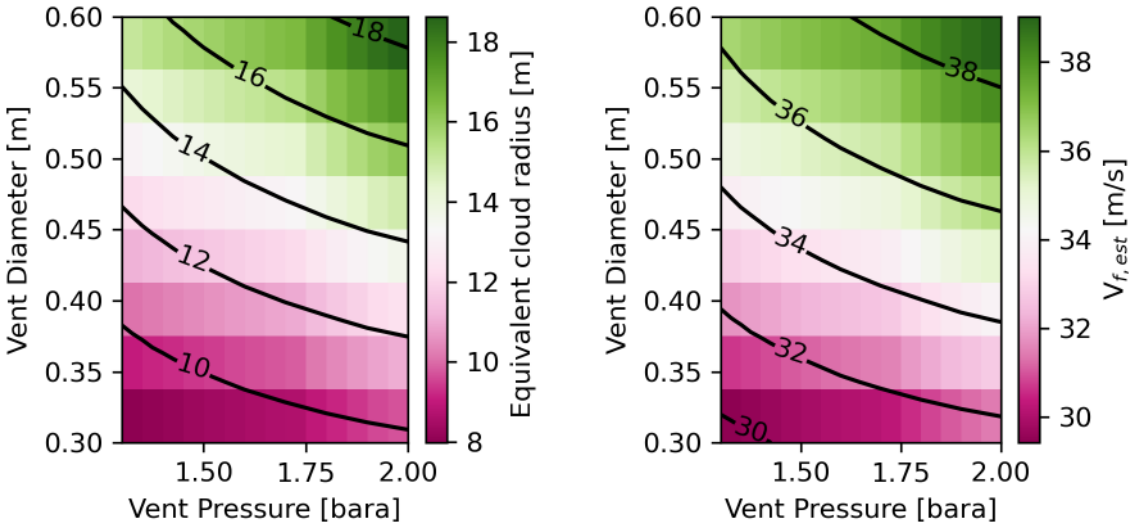

Figure 18 Heat maps show (left) the equivalent cloud radius (m), computed using cloud volume from the dispersion model via Equation 18, and (right) the estimated visible flame speed (m/s), calculated using equivalent cloud radius via Equation 17.

After determination of the visible flame speed, the deflagration overpressure can be calculated, with results presented in Figure 19. For consistency in illustration of overpressures, the same distance (15 m) as used in the detonation case was chosen. It was observed that an increase in both the mass of hydrogen and the cloud size—leading to a higher visible flame speed—results in greater deflagration overpressures. This parametric space yields a deflagration overpressure range of 0.49–1.24 kPa. The potential consequences of deflagration overpressure hazards include loud noise comparable to a sonic boom, occasional glass breakage (0.49 kPa), and reaching pressure levels near the typical threshold for glass breakage (1.24 kPa) [33].

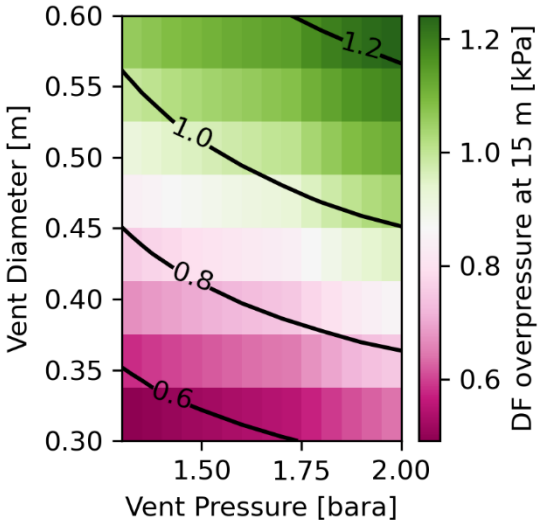

Figure 19 Heat map showing deflagration overpressure estimates at 15 m from the ignition source for combinations of release conditions within the range of $d = 300 - 600\ mm$ *and* $P_{source} = 1.3 - 2\ bara$.

This section presented deflagration and detonation overpressure estimates based on the study's scope of interest, i.e., process venting. The resulting heat maps highlighted the substantial disparity between the two models, further supporting the need—highlighted in the previous validation section—to improve the current methodology in order to narrow the prediction gap. It is rare for detonation to initiate under unconfined and uncongested conditions. Thus, the focus is shifted to improving the deflagration model, while retaining the detonation overpressure as an upper boundary.

8 Towards improved deflagration overpressure model

Following the model validation, the need for improvement in hydrogen gas venting models becomes evident to reduce the prediction error gap. The challenge lies in determining which model requires more urgent refinement. In the field of safety, it is generally preferable to be overly conservative rather than to underestimate, to ensure that no potential hazard and consequences are overlooked, and that effective mitigation is achievable. However, it should not be excessively conservative, as this can lead to unnecessarily costly facility layouts and operations.

The previous validation showed that the detonation model yields conservative estimates. The correlation depends solely on the mass of hydrogen. Improvement can be achieved by redefining the detonability limit, which governs the mass of hydrogen within the dispersed cloud. In fact, it is known that detonation can be unlikely occurred in the uncongested and unconfined industrial circumstances. In this study, therefore, the detonation model can still be retained as an upper bound for overpressure predictions.

The deflagration model can better describe delayed ignition scenarios in hydrogen clouds than detonation, as it also incorporates fundamental combustion properties. However, it has been found that the model mostly underestimates overpressures by an order of magnitude. Improving the deflagration model is more complex, as it primarily depends on two parameters: the mass of hydrogen within the flammable contour and the visible flame speed. Again, estimating the visible flame speed remains a major challenge, since it is not a unique or easily defined value, in reality. Therefore, priority should be given to improving the deflagration model for enhanced prediction accuracies in such scenarios.

The following subsections follow a sensitivity analysis of these two parameters—mass of hydrogen and the visible flame speed—are carried out to determine which one should be the focus of deflagration model improvement in this study. The entire process and reasoning will lead to conclusions on what the study has discovered and what is recommended for improving the accuracy of deflagration overpressure estimates. Finally, the improved predictive performance of the deflagration model will again be assessed in the validation subsection, using the same experimental data from Air Products [32] and Groethe et.al. [7].

8.1 Sensitivity analysis of deflagration model

Based on Equation 16, by keeping the fundamental combustion properties constant, the visible flame speed (V_f) and the mass of hydrogen within the contour limit that contributes to blast loads, are the key parameters for the parametric study of the deflagration model. The analysis enables investigation of how sensitive each parameter is towards the overpressure prediction.

Figure 20 depicts the deflagration overpressure against distances from the ignition point under a fixed set of values: (i) hydrogen mass of 1, 10, and 100 kg and (ii) flame speed of 10, 50, and 250 m/s. The calculation results, considering only the peak overpressure, are listed in Table 6. All FCP remained as averaged values to minimise complexity. While fixing V_f and increasing the hydrogen mass by one and two orders of magnitude, the resulting curves changed only by shifting to the right. In other words, the peak overpressures corresponding to each hydrogen mass yielded around the same magnitude at a fixed V_f, but the locations of the peaks are further away when the masses increase.

As flame speed increases, a corresponding rise in peak overpressure can be observed, following $p_2^* \propto \left(\frac{V_f}{a_0}\right)^2$. An increase in overpressure by a factor of 25 was recorded for all hydrogen gas masses when the visible flame speed increased from 10 to 50 m/s. However, further increasing the flame speed to 250 m/s resulted in a similar magnitude of overpressure increase as that observed from 10 to 50 m/s. This sensitivity analysis on the deflagration model demonstrates that care should be taken to prioritise the investigation of other potential approaches to achieve a more realistic flame speed estimation, enabling sensible prediction of deflagration overpressure. This is because deflagration is aimed to be

the most likely consequence of venting occurring after delayed ignition, followed by flame generation and simultaneously flame acceleration, which is solely responsible for pressure rise.

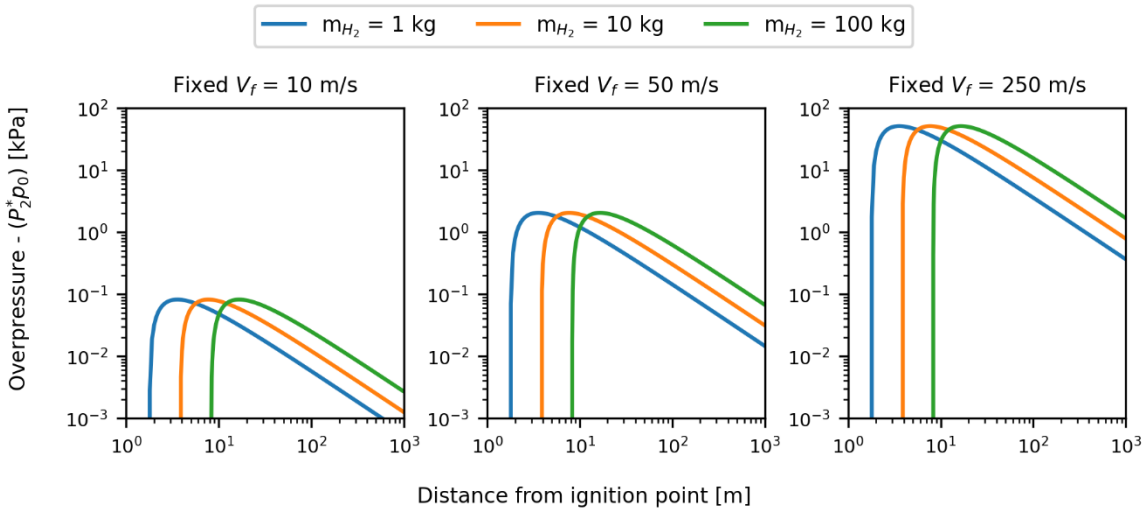

Figure 20 Deflagration overpressure-distance profiles varying hydrogen mass of 1, 10, and 100 kg and visible flame speed of 10, 50, and 250 m/s.

Table 6 Results of sensitivity analysis for the deflagration model considering only peak overpressure values

V_f (m/s)	m_{H_2} (kg)	R (m)	Predicted overpressure $P_2^* P_0$ (kPa)
10	1	3	0.0788
	10	7	0.0809
	100	18	0.0812
50	1	3	1.9692
	10	7	2.0229
	100	18	2.0298
250	1	3	49.2308
	10	7	50.5735
	100	18	50.7452

8.2 Visible flame speed estimation— an improvement strategy

Following the proof previously established in Section 6, it implies that a key challenge is to develop a model that can accommodate the non-uniform and non-quiescent nature of hydrogen jet releases, which is also linked to the need to find a reliable solution to estimate visible flame speed. Available jet release experiments reporting on flame speeds were tested using the previous methodology—to estimates visible flame speed via Equation 17—the correlation was found to underestimate flame speed. This underestimation is one of the root causes of the deflagration overpressure underprediction (see Table 7).

Table 7 Compiled list of V_f estimates based on cloud radius and reported value.

Test configuration	d (mm)	P_{source} (bara)	V_{cloud} (m^3)	R_{cloud} (m)	$V_{f,Rcloud}$ (m/s)	$V_{f,measured}$ (m/s)	Reference
Vertical jet release	42	24	179.4	4.4	24.1	112	[7]
Horizontal jet release	12	40	18.92	2.08	18.76	200	[34]
			18.92	2.08	18.76	510	[34]
			18.92	2.08	18.76	280	[35]
	6	40	2.51	1.06	14.98	120	[36]
			2.51	1.06	14.98	470	[36]
	10	400	373	5.63	26.12	978	[37]

Due to the lack of available experimental data for the condition of interest, i.e., open-atmosphere vertical releases, a set of seven experiments, regardless of hydrogen release direction, has been gathered, and is described in Table 8.

The release conditions in these existing experiments appear to lie outside the initially defined scope of process venting range, which was set at $\mathrm{d} = 300 - 600\ \mathrm{mm}$ and $\mathrm{P_{source}} = 1.3 - 2\ \mathrm{bara}$. However, an alternative means of verification is through the flow regime, assessed using the Reynolds number, which is computed by Equation 19.

$$\mathrm{Re} = \frac{\rho u d}{\mu} \qquad \textit{Equation 19}$$

Where d is vent diameter (m). $\rho, u,$ and μ are hydrogen density (kg/m^3), jet velocity (m/s), and dynamic viscosity (kg/m·s), respectively, which can be extracted from FRED according to a given release condition (a pair of pressure and vent size).

Considering the process venting range of $\mathrm{d} = 300 - 600\ \mathrm{mm}$ and $\mathrm{P_{source}} = 1.3 - 2\ \mathrm{bara}$, the corresponding Reynolds number spans from 2.63×10^6 $(300\ \mathrm{mm}, 1.3\ \mathrm{bara})$ to 9.56×10^6 $(600\ \mathrm{mm}, 2\ \mathrm{bara})$. According to Table 8, the collected experiments yield Reynolds numbers ranging from 1.87×10^6 to 2.42×10^7. Two additional data points from uniform stoichiometric H_2/air mixtures experiments, with hemispherical cloud radii of 3 and 10 m, representing no-flow conditions, are also included. The hydrogen-air density under these quiescent conditions is 0.025 kg/m^3 at normal pressure and temperature (1.013 bara and 25°C).

Based on observations of factors influencing the overpressure, turbulence effects should be noted as important since the condition of interest involves jet releases [35,37]. Therefore, a strategy is to investigate flow regimes of given release conditions (variation of diameter and pressure) through the Reynold numbers and relate that to the visible flame speeds within the experimental range.

Table 8 List of hydrogen deflagration and detonation experiments collected with computed Re.

Test configuration	d (mm)	P_{source} (bara)	$V_{f,measured}$ (m/s)	ρ (kg/m^3)	u (m/s)	$\mu \times 10^3$ (g/m*s)	Computed $Re \times 10^{-6}$	Referen -ce
Vertical jet release	42	24	112	1.168	988.5	6.11	7.93	[7]
Horizontal jet release	12	40	200	1.933	992.6	6.16	3.74	[34]
			510	1.933	992.6	6.16	3.74	[34]
			280	1.933	992.6	6.16	3.74	[35]
	6	40	120	1.933	992.6	6.16	1.87	[36]
			470	1.933	992.6	6.16	1.87	[36]
	10	400	978	16	1098.3	8.53	20.6	[37]
	20.9	60	142.33*	2.875	997.7	6.23	9.63	[38]
			115.92*	2.875	997.7	6.23	9.63	[38]
	52.5	60	299.01*	2.875	997.7	6.23	24.2	[38]
			226.02*	2.875	997.7	6.23	24.2	[38]
Quiescent atmosphere stoichiometric concentration H_2/air cloud	-	1.013	40	0.025	0	-	0	[31]
			80	0.025	0	-	0	[31]

** Flame speeds estimated by fitting the reported overpressure to deflagration correlation (Equation 16)*

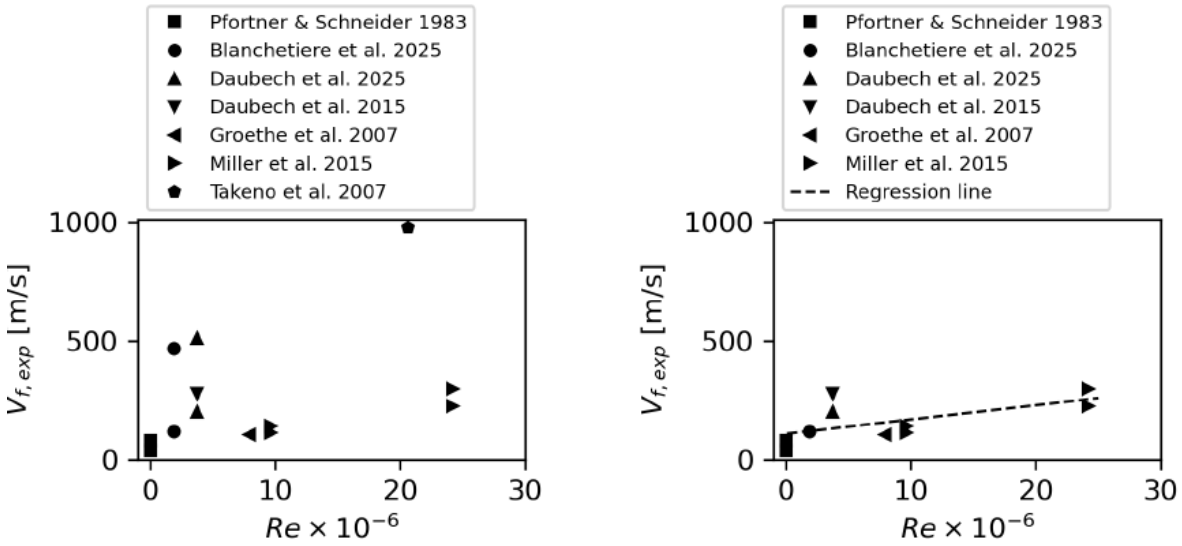

Figure 21 Flame speed plotted against Reynold number. (Left) Untreated plot containing all 7 experiments (Right) Curated data set with least-square linear regression line $V_f = 6.0061(Re \times 10^{-6}) + 110.0135$ *as a dashed line.*

Figure 21 shows the relationship between the visible flame speed and Reynolds number. Figure 21 (left) illustrates a scattered plot of all data points from the experiments listed on Table 8. The experiments are mostly based on horizontal releases. Note that V_f values marked with an asterisk in the table above are flame speeds estimated by fitting the reported overpressure to deflagration correlation (Equation 16). These fitted V_f were included to span a wider range of Reynolds numbers and examine whether they align with the rest of the reported data. A few outliers were identified and

subsequently excluded. Figure 21 (right) shows the curated dataset after three outliers were removed due to the following reasons:

(i) Takeno et.al. [37] reported an extremely high flame speed of 978 m/s (for d = 10 mm and P_{source} = 400 bara), which is more likely represent the gas speed at the vent exit, found to be around 1100 m/s according to FRED simulation (see Table 8).

(ii) Daubech et.al. [34] reported a V_f of 510 m/s which differs significantly from the lead author's previous work 280 m/s under the same release condition (d = 12 mm and P_{source} = 40 bara).

(iii) Blanchetière et.al. [36] conducted tests under similar release condition to Daubech et.al. [34], except with a smaller diameter (d = 6 mm and P_{source} = 40 bara). Hence, the relatively high flame speed of 470 m/s is omitted.

After identifying a potential scaling relationship in the dataset, linear regression was applied to the remaining data points. As a result, an expression for estimating flame speed from the Reynolds number was derived, represented by the dashed line: $V_f = 6.0061(Re \times 10^{-6}) + 110.0135$.

8.3 Validation of improved deflagration model

The approach was first tested against the dataset from Groethe et.al. [7]. The release conditions in this experiment were d = 42 mm and P_{source} = 24 bar. Based on the dispersion model results, the exit velocity was 988.5 m/s, the exit density was 1.168 kg/m³, and the dynamic viscosity was 0.006112 g/(m·s), resulting in a Reynolds number of 7.93×10^6, corresponding to a visible flame speed of 157.67 m/s. The estimated deflagration overpressure from Equation 16 was 15.67 kPa, which is around a factor of 3.9 higher than the reported value of 4 kPa.

The process venting scheme ($d = 300 - 600$ mm and $P_{source} = 1.3 - 2$ bara) provides the combinations of vent diameters and release pressures, producing a wide range of Reynolds numbers from 2.63×10^6 (300 mm, 1.3 bara) to 9.56×10^6 (600 mm, 2 bara), whereas the Air Products data ranges from 3.3×10^5 to 3.0×10^6. The performance of the modified deflagration model can be seen in the figure below.

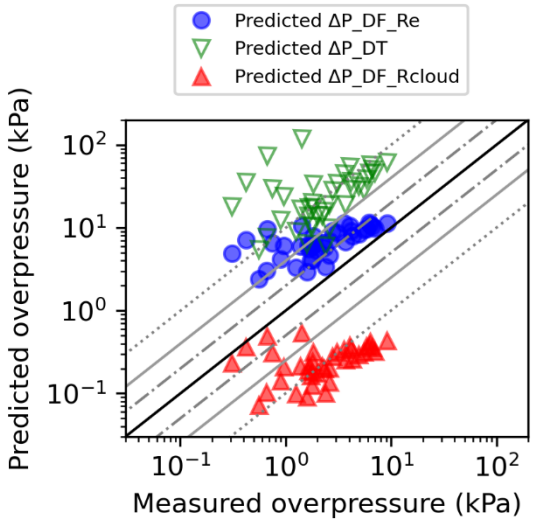

Figure 22 Model performance shown on a log-log scale plot of predicted blast overpressure using three different models against the reported overpressure from Air Products. Red triangles represent overpressure estimates from the deflagration (DF) model. Green downward triangles indicate overpressure estimates from the detonation (DT) model. Blue circles denote deflagration overpressure estimates from the improved flame speed model where $V_f = f(Re)$. Solid black line denotes a perfect match between predicted and experimental

overpressures. Grey dash-dot lines represent a factor of two overestimation and underestimation relative to the reported overpressures. Solid grey lines are guided lines of four-fold overestimation and underestimation. Grey dashed lines serve as an indicator of an order magnitude of overestimation and underestimation.

Figure 22 shows the predicted deflagration and detonation overpressure results for the Air Products experiments, which incorporated a new approach that estimates visible flame speed as a function of Reynolds number, $V_f = f(Re)$. The blue dots represent the predicted overpressures obtained from the improved V_f correlation, plotted alongside the results from the previous deflagration and detonation models. With the improved method for determining visible flame speed, the predictions are more accurate, as the blue dot cluster lies relatively closer to the perfect match line (solid black line) compared to the previous models.

Table 9 summarises the predictive capabilities of the updated deflagration model, categorised by over-/underprediction factor ranges. The previous version of the deflagration model (discussed in Section 6.2), which estimated visible flame speed based on the effective cloud radius, produced only 5 estimates (12.5%) within a factor of four. In contrast, the enhanced deflagration model, using $V_f = f(Re)$, yielded 29 out of 40 predictions (72.5%) within a factor of four. Moreover, the improved model significantly increased the number of predictions within a factor of two—from 3 (7.5%) in the previous model to 13 (32.5%) in the updated version.

Table 9 Model performance summary for the original and updated deflagration models (where visible flame speed is estimated as a function of Reynolds number). The table lists the number of data points falling within each prediction band. The bold number in each prediction band indicates that the interval includes that upper limit.

Prediction bands	**Total 40 data points**	
	Deflagration (Original)	**Deflagration (New)**
>10x	24 (60%)	3 (7.5%)
4x–**10x**	11 (27.5%)	8 (20%)
2x–**4x**	2 (5%)	16 (40%)
1x–**2x**	3 (7.5%)	13 (32.5%)

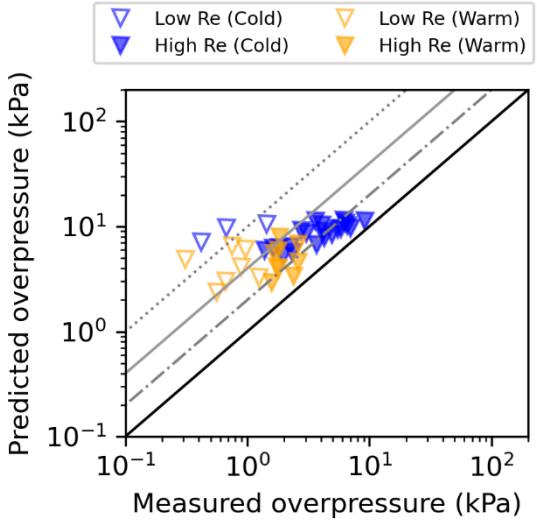

Figure 23 Model performance shown on a log-log scale plot of predicted blast overpressure using improved V_f models against the reported overpressure from Air Products. Unfilled markers denote experiments span the low Reynolds numbers range ($Re \leq 10^6$). Filled markers correspond to high Reynolds numbers test range

($Re > 10^6$). Blue and yellow markers represent cold and warm release tests respectively. Solid black line denotes a perfect match between predicted and experimental overpressures. Light grey line is a guided line of four-fold overestimation relative to the reported overpressures. Grey dash-dot line represents a factor of two overestimation. Dashed line serves as an indicator of an order magnitude of overestimation relative to the reported overpressures.

Looking more closely at the effects of different release conditions, it can be observed that the validity of the improved expression is limited by the Reynolds number range. Figure 23 presents only the overpressure estimates obtained using the improved flame speed correlation. Blue and yellow markers represent cold and warm releases, respectively, further subdivided into high (filled markers) and low (unfilled markers) Reynolds number range denoted as high-Re and low-Re: (i) high-Re tests: Re $> 10^6$, and (ii) low-Re tests: $Re \leq 10^6$.

Table 10 Model performance summary for the updated deflagration model, where visible flame speed is estimated as a function of Reynolds number. The table lists the number of data points falling within each range of overprediction factors sorted by range of Reynolds number.

Prediction bands	Total 10 data points	Total 30 data points
	Low-Re ($Re \leq 10^6$)	**High-Re ($Re > 10^6$)**
>10x	3 (30%)	0 (0%)
4x–**10x**	6 (60%)	2 (7%)
2x–**4x**	1 (10%)	15 (50%)
1x–**2x**	0 (0%)	13 (43%)

For a total of 30 data points corresponding to high-Re releases, the improved approach yields lower prediction errors—93% of the cases remain within a four-fold overestimation for both cold and warm tests. No prediction exceeds an order-of-magnitude overestimation.

However, for low-Reynolds-number (low-Re) cases, 90% of the deflagration overpressure estimates (9 out of 10 data points) still fall within a range exceeding a factor of four, with three reaching more than an order of magnitude overestimation. This indicates that further refinement of the model is required for low-Re flow regimes.

8.4 Heat maps results – updated deflagration model

Previous investigation over the collected experimental dataset illustrated a possible scaling trend relating visible flame speed to the Reynolds number, yielding the expression $V_f = 6.0061(Re \times 10^{-6}) + 110.0135$. The validation in Section 8.3 demonstrated that for Re $> 10^6$, the model provides sufficiently close estimates to the real values, and can be applied within the process venting range of $d = 300 - 600$ mm and $P_{source} = 1.3 - 2$ bara. The corresponding Reynolds number spans from 2.63×10^6 (300 mm, 1.3 bara) to 9.56×10^6 (600 mm, 2 bara).

Incorporating the developed approach for estimating visible flame speed as $V_f = f(Re)$, Figure 24 shows predicted values ranging from 126 to 167 m/s. This enables updated deflagration estimates at 15 m, resulting in values ranging from 9.0 to 22.9 kPa, as shown in Figure 25. The possible consequences [33] from these release conditions fall within in the range of the following:

- 9 kPa–Corrugated asbestos shattered. Corrugated steel or aluminium panels fastenings fail, followed by buckling; wood panel fastenings fail, panels blown in. Personnel are provided a high degree of protection from death or serious injury, with injuries that do occur being principally caused by glass breakage and building debris.
- 22.9 kPa–Frameless, self-framing steel panel building demolished; rupture of oil storage tanks. Personal injuries of a serious nature or possible death are likely from fragments, debris, firebrands, or other objects. There is a 10% chance of eardrum rupture.

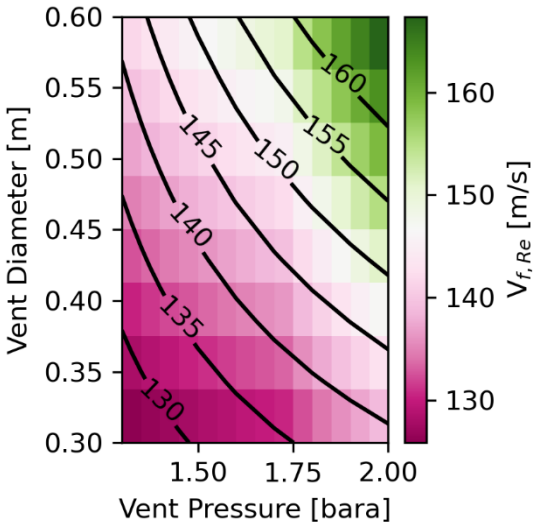

Figure 24 Heat map of visible flame speeds (m/s) estimated using a scaling relationship with Reynolds numbers obtained from experiments, expressed as $V_f = 6.0061(Re \times 10^{-6}) + 110.0135$.

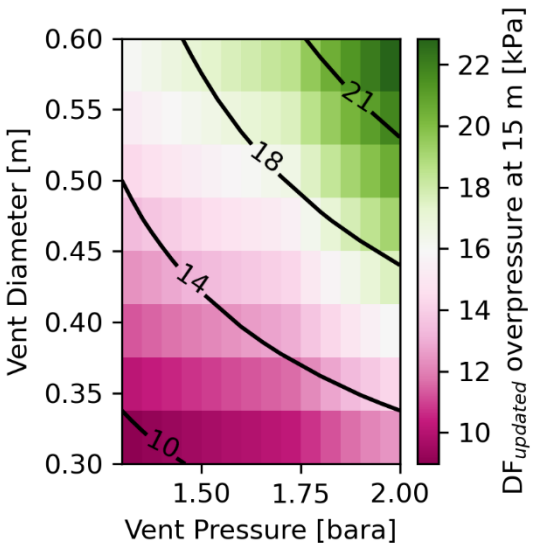

Figure 25 Heat map showing improved deflagration overpressure estimates at 15 m from the ignition source, for release conditions within the parametric range of $d = 300 - 600\ mm$ *and* $P_{source} = 1.3 - 2\ bara$.

The visible flame speed estimates ($V_f = f(Re)$) were found to be approximately 4.2 times higher than those obtained through the original ones (see Figure 18), which based the predictions on equivalent cloud radius. Consequently, this scaling approach increased the deflagration overpressure estimates by approximately 19 times from the original deflagration model.

9 Conclusion

The study was able to reintroduce the methodology Melguizo-Gavilanes et.al. [1] to test the prediction capability of the blast load resulting from hydrogen venting, or more specifically, aimed at the case of delayed ignition of a non-uniform hydrogen cloud in the open atmosphere using deflagration and detonation models. For a given release condition, the deflagration model tends to underestimate the blast load—88% of the 40 predictions underpredict by more than a factor of four—while the detonation correlation yields extremely conservative overpressure values, with 95% of predictions overestimating by more than a factor of four. In the context of safety, overprediction is generally preferable, as the consequences of underestimation are not negligible. This highlights the need to improve the deflagration model, while retaining the detonation overpressure as a conservative upper bound.

A sensitivity analysis was conducted to investigate the most sensitive parameter for the deflagration model. The visible flame speed has the strongest impact on the deflagration correlation. Obtaining direct measurements of visible flame speeds poses a significant challenge given the fact that it is not a single value but varies depending on the different concentrations of hydrogen in different locations within a gas cloud. According to Section 8.2, estimating the flame speed as a function of cloud radius and FCP appears to result in a relatively slower flame speed than what is reported. Alternatively, a new approach is to estimate the flame speed by the Reynolds number, as gas release under pressure will generate turbulent flow. The experimental flame speed under different release conditions, regardless of release direction, was collected, screened, and plotted against the Reynolds number, which can be analytically calculated based on results from the FRED simulation. A regression was then obtained and tested against the vertical hydrogen release experiments. The updated flame speed estimates provided improvements in overpressure prediction for the deflagration model, as they brought the estimates closer to the measured overpressures, showing better performance. Out of 40 predictions, 73% resulted in less than a factor of four overestimation, and 33% of all predictions were within a factor of two.

10 Future work

Based on the updated methodology performance in Section 8.3, there remains scope for further improvement for deflagration model. One area is the refinement of the updated flame speed correlation to better accommodate the lower Reynolds number range ($Re \leq 10^6$). As mentioned in Figure 21, the data representing $Re = 0$ correspond to an idealised set of conditions, categorised as quiescent and uniform stoichiometric concentration tests, which represent the most reactive conditions, resulting in a higher flame speed. In contrast, the study's situation of interest involves a non-uniform cloud, where the flame speed can vary across different locations and is expected to be lower than that observed in the uniformity tests included in the regression, which represent an upper threshold of flame speed. The high V_f at $Re = 0$ influences the regression line, leading to higher flame speed predictions and, consequently, overpredictions of overpressure. Hence, visible flame speed data at lower flame speed and Reynolds number for non-uniform concentrations are needed, and the corresponding flame speeds are expected to be lower—below 80 m/s. Furthermore, there is a need to broaden the experimental campaign to extend the range of Reynolds numbers tested and assess the model's validity under a wider variety of release conditions, as current validation has only been carried out within a relatively narrow Reynolds number range of 3.3×10^5 to 7.93×10^6.

Lastly, for the detonation model, elimination of overconservative overpressure estimates requires reassessing the detonability contour limit to properly define the mass of the gas cloud contributing to the blast. This would subsequently enable more realistic detonation overpressure estimation.

11 References

[1] Melguizo-Gavilanes J, Pekalski A, Crerand A. A methodology for hydrogen vents overpressure assessments, Hazards 34 Process Safety Conference, Manchester, UK: 2024.

[2] Energy Agency I. Global Hydrogen Review 2024 2024.

[3] Guide to Safety of Hydrogen and Hydrogen Systems (ANSI/AIAA G-095A-2017). Guide to Safety of Hydrogen and Hydrogen Systems (ANSI/AIAA G-095A-2017) 2017. https://doi.org/10.2514/4.105197.001.

[4] Boivin P, Le Boursicaud M, Millán-Merino A, Taileb S, Melguizo-Gavilanes J, Williams F. Hydrogen ignition and safety n.d. https://doi.org/10.1007/978-3-031-28412-0_5ï.

[5] Hu Q, Zhang X, Hao H. A review of hydrogen-air cloud explosions: The fundamentals, overpressure prediction methods, and influencing factors. Int J Hydrogen Energy 2023;48:13705–30. https://doi.org/10.1016/J.IJHYDENE.2022.11.302.

[6] Astbury GR, Hawksworth. SPONTANEOUS IGNITION OF HYDROGEN LEAKS: A REVIEW OF POSTULATED MECHANISMS. n.d.

[7] Groethe M, Merilo E, Colton J, Chiba S, Sato Y, Iwabuchi H. Large-scale hydrogen deflagrations and detonations. Int J Hydrogen Energy 2007;32:2125–33. https://doi.org/10.1016/J.IJHYDENE.2007.04.016.

[8] Miller D, Eastwood CD, Thomas JK. Hydrogen jet vapor cloud explosion: test data and comparison with predictions. Proceedings of the 11th Global Congress on Process Safety, AIChE Annual Meeting, Austin, TX, 2015, p. 26–30.

[9] American Petroleum Institute. API Standard. Pressure-relieving and depressuring systems. 2020.

[10] Melton TA, Marx JD. Estimating Flame Speeds for Use with the BST Blast Curves. n.d.

[11] Ahlert RC. Guidelines for consequence analysis of chemical releases. Center for Chemical Process Safety, American Institute of Chemical Engineers (AIChE), New York, NY, (1999,) 320 Pages, [ISBN No.: 0-8169-0786-2], US. List Price: $129.00. Environmental Progress 2000;19. https://doi.org/10.1002/EP.670190304.

[12] Van Den Berg AC. THE MULTI-ENERGY METHOD A FRAMEWORK FOR VAPOUR CLOUD EXPLOSION BLAST PREDICTION. n.d.

[13] Pierorazio AJ, Thomas JK, Baker QA, Ketchum DE. An Update to the Baker-Strehlow-Tang Vapor Cloud Explosion Prediction Methodology Flame Speed Table 2004.

[14] Baker QA, Tang MJ, Scheier EA, Silva GJ. Vapor cloud explosion analysis. Process Safety Progress 1996;15:106–9. https://doi.org/10.1002/PRS.680150211.

[15] Mukhim ED, Abbasi T, Tauseef SM, Abbasi SA. A method for the estimation of overpressure generated by open air hydrogen explosions. J Loss Prev Process Ind 2018;52:99–107. https://doi.org/10.1016/j.jlp.2018.01.009.

[16] Mueschke NJ, Joyce A. Measurement of gas detonation blast loads in semiconfined geometry. J Loss Prev Process Ind 2020;63. https://doi.org/10.1016/j.jlp.2019.104004.

[17] Dorofeev SB. Evaluation of safety distances related to unconfined hydrogen explosions. Int J Hydrogen Energy 2007;32:2118–24. https://doi.org/10.1016/j.ijhydene.2007.04.003.

[18] Thomas JK, Eastwood C, Goodrich M. Are unconfined hydrogen vapor cloud explosions credible? Process Safety Progress 2015;34:36–43. https://doi.org/10.1002/prs.11685.

[19] Reider R, Otway HJ, Knight HT. AN UNCONFINED LARGE-VOLUME HYDROGEN-AIR EXPLOSION, Los Alamos National Lab.(LANL), Los Alamos, NM (United States); Los Alamos …; 1962.

[20] Reider R, Otway H, Knight H. An unconfined, large-volume hydrogen/air explosion. AEC-NASA Tech Brief 1971;71.

[21] Ordin PM. Review of hydrogen accidents and incidents in NASA operations. National Aeronautics and Space Administration; 1974.

[22] Ciccarelli G, Dorofeev S. Flame acceleration and transition to detonation in ducts. Prog Energy Combust Sci 2008;34:499–550. https://doi.org/10.1016/J.PECS.2007.11.002.

[23] Dorofeev SB. Flame acceleration and explosion safety applications. Proceedings of the Combustion Institute 2011;33:2161–75. https://doi.org/10.1016/J.PROCI.2010.09.008.

[24] Molkov V V., Makarov D V., Schneider H. Hydrogen-air deflagrations in open atmosphere: Large eddy simulation analysis of experimental data. Int J Hydrogen Energy 2007;32:2198–205. https://doi.org/10.1016/j.ijhydene.2007.04.021.

[25] Johnson DM, Allason D, Cronin PM. Large scale experimental research of VCEs – A summary from one viewpoint. J Loss Prev Process Ind 2024;89:105287. https://doi.org/10.1016/J.JLP.2024.105287.

[26] Shell FRED 2025 Technical Guide. 2025.

[27] HGSYSTEM n.d. http://www.hgsystem.com/hgweb.html (accessed May 15, 2025).

[28] A. GF. Use of routine meteorological observations for estimating atmospheric dispersion. Nucl Safety 1961;2:47–51.

[29] Bauwens CRL, Dorofeev SB. Modeling detonation limits for arbitrary non-uniform concentration distributions in fuel–air mixtures. Combust Flame 2020;221:338–45. https://doi.org/10.1016/j.combustflame.2020.08.003.

[30] Kaneshige M, Shepherd JE. Detonation database. 1997.

[31] Schneider H, Pförtner H. PNPSichcrheitssofortprogramm, Prozebgasfreisetzung-Explosion in der Gasfabrik und Auswirkungen von Druckwellen auf das Containment. 1983.

[32] Shen C, Miller D, Lutostansky E, Overa S, Malik D, Macon K, et al. Hydrogen Jet Explosion: New Tests, Blast and Fireball Models. 2025.

[33] Casal J. Evaluation of the Effects and Consequences of Major Accidents in Industrial Plants. Industrial Safety Series 2008;8:61–117.

[34] Daubech J, Hebrard J, Leprette E. Influence of the flammable cloud geometry on the gas explosion effects. Process Safety Progress 2025. https://doi.org/10.1002/prs.12674.

[35] Daubech J, Hebrard J, Jallais S, Vyazmina E, Jamois D, Verbecke F. Un-ignited and ignited high pressure hydrogen releases: Concentration - Turbulence mapping and overpressure effects. J Loss Prev Process Ind 2014;36:439–46. https://doi.org/10.1016/j.jlp.2015.05.013.

[36] Blanchetière V, Armstrong A, Wang Y, Jambut R, Wilkins B, Salaün N. Delayed ignition of high-pressure hydrogen releases – Experiments and engineering models. J Loss Prev Process Ind 2025;94. https://doi.org/10.1016/j.jlp.2025.105589.

[37] Takeno K, Okabayashi K, Kouchi A, Nonaka T, Hashiguchi K, Chitose K. Dispersion and explosion field tests for 40 MPa pressurized hydrogen. Int J Hydrogen Energy 2007;32:2144–53. https://doi.org/10.1016/j.ijhydene.2007.04.018.

[38] Jallais S, Vyazmina E, Miller D, Thomas JK. Hydrogen jet vapor cloud explosion: A model for predicting blast size and application to risk assessment. Process Safety Progress 2018;37:397–410. https://doi.org/10.1002/prs.11965.

Annex A

A1. Air Product Validation results

Appendix Table 1 Relevant reported data for selected warm and cold releases.

Test code	$T_{release}$	d (mm)	$\dot{m}_{H_2}$ (kg/s)	R (m)	Reported overpressure (kPa)
A05	277	101.6	0.15	11.02	1.25
A05	277	101.6	0.15	15.65	0.56
A07	277	101.6	0.25	6.93	0.96
A07	277	101.6	0.25	11.02	0.89
A07	277	101.6	0.25	15.65	0.66
A09	254	101.6	0.46	6.93	1.79
A09	254	101.6	0.46	11.02	1.79
A09	254	101.6	0.46	15.65	1.59
A10	258	101.6	0.49	6.93	1.84
A10	258	101.6	0.49	11.02	1.67
A10	258	101.6	0.49	15.65	1.74
A12	261	50.8	0.46	6.93	2.6
A12	261	50.8	0.46	11.02	2.6
A12	261	50.8	0.46	15.65	2.38
A14	246	203.2	0.49	11.02	0.75
A14	246	203.2	0.49	15.65	0.31
B06	190	203.2	0.47	4.80	1.43
B06	190	203.2	0.47	6.60	0.67
B06	190	203.2	0.47	10.86	0.42
B07	161	50.8	0.57	4.80	3.6

Test code	$T_{release}$	d (mm)	$\dot{m}_{H_2}$ (kg/s)	R (m)	Reported overpressure (kPa)
B07	161	50.8	0.57	6.60	2.78
B07	161	50.8	0.57	10.86	1.63
B10	175	50.8	0.55	4.80	6.16
B10	175	50.8	0.55	6.60	5.52
B10	175	50.8	0.55	10.86	2.24
B11	155	76.2	0.56	4.80	9.13
B11	155	76.2	0.56	6.60	5.87
B11	155	76.2	0.56	10.86	3.69
B12	172	76.2	0.52	4.80	7.05
B12	172	76.2	0.52	6.60	4.28
B12	172	76.2	0.52	10.86	2
B13	180	76.2	0.53	4.80	6.64
B13	180	76.2	0.53	6.60	4.92
B13	180	76.2	0.53	10.86	2.32
B14	175	76.2	0.52	4.80	6.36
B14	175	76.2	0.52	6.60	4.2
B14	175	76.2	0.52	10.86	1.8
B15	170	76.2	0.5	4.80	4.07
B15	170	76.2	0.5	6.60	3.06
B15	170	76.2	0.5	10.86	1.39

Appendix Table 2 Relevant data for selected warm and cold releases used in the calculation of overpressures and predicted overpressures using deflagration model, where visible flame speeds were estimated using Equation 17. The values of P_{source}, V_{cloud}, and m_{H_2} were obtained from FRED.

Test code	$T_{release}$	d (mm)	$\dot{m}_{H_2}$ (kg/s)	P_{source} (bara)	V_{cloud} (m^3)	R_{cloud} (m)	$V_{f,Rcloud}$ (m/s)	m_{H_2} (kg)	R (m)	Predicted overpressure $P_2^* P_0$ (kPa)
A05	277	101.6	0.15	1.044	25.41	2.30	19.38	0.1623	11.02	0.099
A05	277	101.6	0.15	1.044	25.41	2.30	19.38	0.1623	15.65	0.072
A07	277	101.6	0.25	1.01	51.18	2.90	20.95	0.3216	6.93	0.208
A07	277	101.6	0.25	1.01	51.18	2.90	20.95	0.3216	11.02	0.141
A07	277	101.6	0.25	1.01	51.18	2.90	20.95	0.3216	15.65	0.103
A09	254	101.6	0.46	1.3	40.58	2.69	20.41	0.2467	6.93	0.184
A09	254	101.6	0.46	1.3	40.58	2.69	20.41	0.2467	11.02	0.124
A09	254	101.6	0.46	1.3	40.58	2.69	20.41	0.2467	15.65	0.090
A10	258	101.6	0.49	1.346	123.4	3.89	23.10	0.75	6.93	0.313
A10	258	101.6	0.49	1.346	123.4	3.89	23.10	0.75	11.02	0.219
A10	258	101.6	0.49	1.346	123.4	3.89	23.10	0.75	15.65	0.162
A12	261	50.8	0.46	4.705	51.31	2.90	20.95	0.2923	6.93	0.203
A12	261	50.8	0.46	4.705	51.31	2.90	20.95	0.2923	11.02	0.138
A12	261	50.8	0.46	4.705	51.31	2.90	20.95	0.2923	15.65	0.100
A14	246	203.2	0.49	1.031	236.8	4.84	24.83	1.648	11.02	0.312
A14	246	203.2	0.49	1.031	236.8	4.84	24.83	1.648	15.65	0.235
B06	190	203.2	0.47	1.026	309.9	5.29	25.59	2.251	4.80	0.535
B06	190	203.2	0.47	1.026	309.9	5.29	25.59	2.251	6.60	0.489
B06	190	203.2	0.47	1.026	309.9	5.29	25.59	2.251	10.86	0.362
B07	161	50.8	0.57	4.557	88.64	3.48	22.27	0.532	4.80	0.341
B07	161	50.8	0.57	4.557	88.64	3.48	22.27	0.532	6.60	0.277
B07	161	50.8	0.57	4.557	88.64	3.48	22.27	0.532	10.86	0.187
B10	175	50.8	0.55	4.631	118.4	3.84	22.99	0.6762	4.80	0.380
B10	175	50.8	0.55	4.631	118.4	3.84	22.99	0.6762	6.60	0.313

Test code	$T_{release}$	d (mm)	$\dot{m}_{H_2}$ (kg/s)	P_{source} (bara)	V_{cloud} (m^3)	R_{cloud} (m)	$V_{f,Rcloud}$ (m/s)	m_{H_2} (kg)	R (m)	Predicted overpressure $P_2^* P_0$ (kPa)
B10	175	50.8	0.55	4.631	118.4	3.84	22.99	0.6762	10.86	0.213
B11	155	76.2	0.56	1.963	166.4	4.30	23.88	1.009	4.80	0.436
B11	155	76.2	0.56	1.963	166.4	4.30	23.88	1.009	6.60	0.368
B11	155	76.2	0.56	1.963	166.4	4.30	23.88	1.009	10.86	0.257
B12	172	76.2	0.52	1.922	74.98	3.30	21.85	0.4682	4.80	0.320
B12	172	76.2	0.52	1.922	74.98	3.30	21.85	0.4682	6.60	0.259
B12	172	76.2	0.52	1.922	74.98	3.30	21.85	0.4682	10.86	0.174
B13	180	76.2	0.53	1.998	99.44	3.62	22.55	0.6118	4.80	0.359
B13	180	76.2	0.53	1.998	99.44	3.62	22.55	0.6118	6.60	0.294
B13	180	76.2	0.53	1.998	99.44	3.62	22.55	0.6118	10.86	0.200
B14	175	76.2	0.52	1.936	146.8	4.12	23.55	0.8803	4.80	0.416
B14	175	76.2	0.52	1.936	146.8	4.12	23.55	0.8803	6.60	0.348
B14	175	76.2	0.52	1.936	146.8	4.12	23.55	0.8803	10.86	0.241
B15	170	76.2	0.5	1.816	114.5	3.80	22.91	0.7093	4.80	0.380
B15	170	76.2	0.5	1.816	114.5	3.80	22.91	0.7093	6.60	0.314
B15	170	76.2	0.5	1.816	114.5	3.80	22.91	0.7093	10.86	0.215

Appendix Table 3 Relevant data for selected warm and cold releases used in the calculation of overpressures and predicted overpressures using detonation model. The values of P_{source} and m_{H_2} were obtained from FRED.

Test code	$T_{release}$	d (mm)	$\dot{m}_{H_2}$ (kg/s)	P_{source} (bara)	m_{H_2} (kg)	R (m)	Predicted overpressure $P_1^* P_0$ (kPa)
A05	277	101.6	0.15	1.044	0.04465	11.02	8.93
A05	277	101.6	0.15	1.044	0.04465	15.65	5.50
A07	277	101.6	0.25	1.01	0.0896	6.93	23.76
A07	277	101.6	0.25	1.01	0.0896	11.02	12.35
A07	277	101.6	0.25	1.01	0.0896	15.65	7.58
A09	254	101.6	0.46	1.3	0.06193	6.93	19.95
A09	254	101.6	0.46	1.3	0.06193	11.02	10.40
A09	254	101.6	0.46	1.3	0.06193	15.65	6.39
A10	258	101.6	0.49	1.346	0.1831	6.93	33.41
A10	258	101.6	0.49	1.346	0.1831	11.02	17.26
A10	258	101.6	0.49	1.346	0.1831	15.65	10.55
A12	261	50.8	0.46	4.705	0.05598	6.93	19.03
A12	261	50.8	0.46	4.705	0.05598	11.02	9.92
A12	261	50.8	0.46	4.705	0.05598	15.65	6.10
A14	246	203.2	0.49	1.031	0.5618	11.02	29.35
A14	246	203.2	0.49	1.031	0.5618	15.65	17.83
B06	190	203.2	0.47	1.026	0.8034	4.80	118.81
B06	190	203.2	0.47	1.026	0.8034	6.60	73.63
B06	190	203.2	0.47	1.026	0.8034	10.86	35.61
B07	161	50.8	0.57	4.557	0.1094	4.80	44.30
B07	161	50.8	0.57	4.557	0.1094	6.60	27.99
B07	161	50.8	0.57	4.557	0.1094	10.86	13.85
B10	175	50.8	0.55	4.631	0.1134	4.80	45.07
B10	175	50.8	0.55	4.631	0.1134	6.60	28.48

Test code	$T_{release}$	d (mm)	$\dot{m}_{H_2}$ (kg/s)	P_{source} (bara)	m_{H_2} (kg)	R (m)	Predicted overpressure $P_1^* P_0$ (kPa)
B10	175	50.8	0.55	4.631	0.1134	10.86	14.08
B11	155	76.2	0.56	1.963	0.2152	4.80	61.60
B11	155	76.2	0.56	1.963	0.2152	6.60	38.71
B11	155	76.2	0.56	1.963	0.2152	10.86	19.03
B12	172	76.2	0.52	1.922	0.1184	4.80	46.03
B12	172	76.2	0.52	1.922	0.1184	6.60	29.07
B12	172	76.2	0.52	1.922	0.1184	10.86	14.37
B13	180	76.2	0.53	1.998	0.144	4.80	50.62
B13	180	76.2	0.53	1.998	0.144	6.60	31.92
B13	180	76.2	0.53	1.998	0.144	10.86	15.75
B14	175	76.2	0.52	1.936	0.1821	4.80	56.76
B14	175	76.2	0.52	1.936	0.1821	6.60	35.73
B14	175	76.2	0.52	1.936	0.1821	10.86	17.59
B15	170	76.2	0.5	1.816	0.1653	4.80	54.14
B15	170	76.2	0.5	1.816	0.1653	6.60	34.10
B15	170	76.2	0.5	1.816	0.1653	10.86	16.81

Appendix Table 4 Relevant data for selected warm and cold releases used in the calculation of overpressures and predicted overpressures using deflagration model, where visible flame speeds were estimated from a least-square regression line given as a function of Reynold number ($V_f = 6.0061(Re \times 10^{-6}) + 110.0135$). The values of P_{source}, exit density, viscosity, exit velocity, and m_{H_2} were obtained from FRED.

Test code	$T_{release}$	d (mm)	$\dot{m}_{H_2}$ (kg/s)	P_{source} (bara)	Exit density (kg/m3)	Viscosity (g/(m*s))	Exit velocity (m/s)	$Re \times 10^{-6}$	$V_{f,Re}$ (m/s)	m_{H_2}(kg)	R (m)	Predicted overpressure (kPa)
A05	277	101.6	0.15	1.044	0.08847	0.005716	209.2	0.329	111.99	0.1623	11.02	3.300
A05	277	101.6	0.15	1.044	0.08847	0.005716	209.2	0.329	111.99	0.1623	15.65	2.391
A07	277	101.6	0.25	1.01	0.08824	0.005768	349.5	0.543	113.28	0.3216	6.93	6.093
A07	277	101.6	0.25	1.01	0.08824	0.005768	349.5	0.543	113.28	0.3216	11.02	4.136
A07	277	101.6	0.25	1.01	0.08824	0.005768	349.5	0.543	113.28	0.3216	15.65	3.020
A09	254	101.6	0.46	1.3	0.09602	0.005664	591	1.018	116.13	0.2467	6.93	5.969
A09	254	101.6	0.46	1.3	0.09602	0.005664	591	1.018	116.13	0.2467	11.02	4.021
A09	254	101.6	0.46	1.3	0.09602	0.005664	591	1.018	116.13	0.2467	15.65	2.926
A10	258	101.6	0.49	1.346	0.09524	0.005716	634.7	1.074	116.47	0.75	6.93	7.946
A10	258	101.6	0.49	1.346	0.09524	0.005716	634.7	1.074	116.47	0.75	11.02	5.562
A10	258	101.6	0.49	1.346	0.09524	0.005716	634.7	1.074	116.47	0.75	15.65	4.117
A12	261	50.8	0.46	4.705	0.2308	0.006061	983.5	1.903	121.44	0.2923	6.93	6.830
A12	261	50.8	0.46	4.705	0.2308	0.006061	983.5	1.903	121.44	0.2923	11.02	4.623
A12	261	50.8	0.46	4.705	0.2308	0.006061	983.5	1.903	121.44	0.2923	15.65	3.371
A14	246	203.2	0.49	1.031	0.09994	0.005359	151.3	0.573	113.46	1.648	11.02	6.507
A14	246	203.2	0.49	1.031	0.09994	0.005359	151.3	0.573	113.46	1.648	15.65	4.903
B06	190	203.2	0.47	1.026	0.1298	0.004678	111.8	0.630	113.80	2.251	4.80	10.575
B06	190	203.2	0.47	1.026	0.1298	0.004678	111.8	0.630	113.80	2.251	6.60	9.681

Test code	$T_{release}$	d (mm)	$\dot{m}_{H_2}$ (kg/s)	P_{source} (bara)	Exit density (kg/m3)	Viscosity (g/(m*s))	Exit velocity (m/s)	$Re \times 10^{-6}$	$V_{f,Re}$ (m/s)	m_{H_2}(kg)	R (m)	Predicted overpressure (kPa)
B06	190	203.2	0.47	1.026	0.1298	0.004678	111.8	0.630	113.80	2.251	10.86	7.154
B07	161	50.8	0.57	4.557	0.3603	0.004755	780.5	3.004	128.06	0.532	4.80	11.279
B07	161	50.8	0.57	4.557	0.3603	0.004755	780.5	3.004	128.06	0.532	6.60	9.166
B07	161	50.8	0.57	4.557	0.3603	0.004755	780.5	3.004	128.06	0.532	10.86	6.188
B10	175	50.8	0.55	4.631	0.3316	0.005	818.3	2.757	126.57	0.6762	4.80	11.507
B10	175	50.8	0.55	4.631	0.3316	0.005	818.3	2.757	126.57	0.6762	6.60	9.474
B10	175	50.8	0.55	4.631	0.3316	0.005	818.3	2.757	126.57	0.6762	10.86	6.465
B11	155	76.2	0.56	1.963	0.1594	0.004682	770.3	1.998	122.02	1.009	4.80	11.376
B11	155	76.2	0.56	1.963	0.1594	0.004682	770.3	1.998	122.02	1.009	6.60	9.614
B11	155	76.2	0.56	1.963	0.1594	0.004682	770.3	1.998	122.02	1.009	10.86	6.700
B12	172	76.2	0.52	1.922	0.1419	0.004931	803.5	1.762	120.60	0.4682	4.80	9.758
B12	172	76.2	0.52	1.922	0.1419	0.004931	803.5	1.762	120.60	0.4682	6.60	7.881
B12	172	76.2	0.52	1.922	0.1419	0.004931	803.5	1.762	120.60	0.4682	10.86	5.293
B13	180	76.2	0.53	1.998	0.1412	0.005028	823.2	1.762	120.59	0.6118	4.80	10.264
B13	180	76.2	0.53	1.998	0.1412	0.005028	823.2	1.762	120.59	0.6118	6.60	8.403
B13	180	76.2	0.53	1.998	0.1412	0.005028	823.2	1.762	120.59	0.6118	10.86	5.708
B14	175	76.2	0.52	1.936	0.1402	0.004967	813.6	1.750	120.52	0.8803	4.80	10.886
B14	175	76.2	0.52	1.936	0.1402	0.004967	813.6	1.750	120.52	0.8803	6.60	9.111
B14	175	76.2	0.52	1.936	0.1402	0.004967	813.6	1.750	120.52	0.8803	10.86	6.302
B15	170	76.2	0.5	1.816	0.1452	0.004833	755.1	1.729	120.40	0.7093	4.80	10.497

Test code	$T_{release}$	d (mm)	$\dot{m}_{H_2}$ (kg/s)	P_{source} (bara)	Exit density (kg/m3)	Viscosity (g/(m*s))	Exit velocity (m/s)	$Re \times 10^{-6}$	$V_{f,Re}$ (m/s)	m_{H_2}(kg)	R (m)	Predicted overpressure (kPa)
B15	170	76.2	0.5	1.816	0.1452	0.004833	755.1	1.729	120.40	0.7093	6.60	8.666
B15	170	76.2	0.5	1.816	0.1452	0.004833	755.1	1.729	120.40	0.7093	10.86	5.927